Annu. Rev. Physiol. 2004. 66:689–733
doi: 10.1146/annurev.physiol.66.032102.150251

First published online as a Review in Advance on November 3, 2003

THE CYTOCHROME BC_1 COMPLEX: Function in the Context of Structure

Antony R. Crofts
Department of Biochemistry, and Center for Biophysics and Computational Biology, University of Illinois at Urbana-Champaign, Urbana, Illinois 61801; email: a-crofts@life.uiuc.edu

Key Words antimycin, stigmatellin, myxothiazol, superoxide, mechanism

■ **Abstract** The bc_1 complexes are intrinsic membrane proteins that catalyze the oxidation of ubihydroquinone and the reduction of cytochrome *c* in mitochondrial respiratory chains and bacterial photosynthetic and respiratory chains. The bc_1 complex operates through a Q-cycle mechanism that couples electron transfer to generation of the proton gradient that drives ATP synthesis.

Genetic defects leading to mutations in proteins of the respiratory chain, including the subunits of the bc_1 complex, result in mitochondrial myopathies, many of which are a direct result of dysfunction at catalytic sites. Some myopathies, especially those in the cytochrome *b* subunit, exacerbate free-radical damage by enhancing superoxide production at the ubihydroquinone oxidation site. This bypass reaction appears to be an unavoidable feature of the reaction mechanism. Cellular aging is largely attributable to damage to DNA and proteins from the reactive oxygen species arising from superoxide and is a major contributing factor in many diseases of old age. An understanding of the mechanism of the bc_1 complex is therefore central to our understanding of the aging process. In addition, a wide range of inhibitors that mimic the quinone substrates are finding important applications in clinical therapy and agronomy. Recent structural studies have shown how many of these inhibitors bind, and have provided important clues to the mechanism of action and the basis of resistance through mutation.

This paper reviews recent advances in our understanding of the mechanism of the bc_1 complex and their relation to these physiologically important issues in the context of the structural information available.

INTRODUCTION

Enzymes of the cytochrome (cyt) bc_1 complex family are central components of all the main energy transduction systems of the biosphere, accounting, through

maintenance of the proton gradient, for ~30% of energy transmission.[1] They all catalyze essentially the same reaction, the transfer of reducing equivalents from a quinol in the lipid phase (ubihydroquinone in the classical bc_1 complexes) to a higher-potential acceptor protein in the aqueous phase. This electron transfer is coupled to transfer of 1 H^+/e^- across the membrane. From an anthropocentric perspective, the mitochondrial complexes are of greatest interest, and the central role in the respiratory chain places them at the heart of cellular physiological function (1–4). The mitochondrial complexes arose from bacterial antecedents, and the catalytic core of three subunits [cyt c_1, cyt *b* and the Rieske iron sulfur protein (ISP)] is highly conserved (5–7). The latter two subunits span the archaeal/bacterial divide and are clearly more ancient than the cyt c_1 subunit, whose function is carried by a wide variety of different structures (3, 6). Because of the greater experimental flexibility, the bc_1 complexes from photosynthetic bacteria have proved useful models for the mitochondrial complexes, especially in kinetic studies. In these studies, the reactions of the complex in situ can be studied following photoactivation of the photosynthetic reaction center (RC), which generates both substrates in <1 ms, allowing better time resolution than is possible using rapid mixing.

Apart from the general philosophical interest, applications in the health and agronomical sciences arise from the central involvement of the complex in cellular energy metabolism and the many ways in which dysfunctions in this role impinge on physiological function.

A wide range of mitochondrial myopathies (using an extended definition that includes related disorders) have been located to mutations in genes encoding the proteins of the bc_1 complex (8–11). The general and specific symptoms of these myopathies provide abundant evidence of the central importance of the complex in energy metabolism. Many myopathies have been characterized at a molecular level, and many of the mutations have been reproduced in yeast or bacterial model systems for more detailed investigation (8, 9). In general, the mapping of lesions to the catalytic interfaces and demonstration of direct effects on catalytic function have provided a deeper understanding of the molecular basis of these important diseases.

---

[1]*Abbreviations*: bc_1 complex, ubiquinol:cytochrome c oxidoreductase (EC 1.10.2.2); b_L and b_H, low- and high-potential hemes of cytochrome *b*, respectively; cyt, cytochrome; $E_{m,(pH)}$, midpoint redox potential at pH indicated (pH 7 assumed if not indicated); $E_{h,(pH)}$, ambient redox potential at pH indicated; ESEEM, electron spin echo envelope modulation spectroscopy; HYSCORE, hyperfine sublevel correlation spectroscopy; HHDBT, 5-heptyl-6-hydroxy-4,7-dioxobenzothiazol; ISP, Rieske iron-sulfur protein; ISPH, reduced ISP; ISP_{ox}, oxidized, dissociated ISP; NQNO, 2-nonyl-4-hydroxyquinoline N-oxide; P^+/P, reaction center primary donor couple, $(BChl_2)^+/(BChl_2)$; P-phase, N-phase, aqueous phases in which the proton gradient is positive or negative, respectively; Q, oxidized form of quinone; QH_2, reduced form (hydroquinone, quinol) of quinone; $QH^\bullet$, $Q^{\bullet-}$, protonated and deprotonated forms of semiquinone; Qi-site (Q_o site), quinone reducing (quinol oxidizing) site of bc_1 complex; *Rb*., *Rhodobacter*; RC, photosynthetic reaction center; SQ, semiquinone (with protonation state unspecified); UHDBT, 5-undecyl-6-hydroxy-4,7-dioxobenzothiazol; UHNQ, 2-undecyl-3-hydroxy-1,4-naphthoquinone.

The Q_o-site of the complex is an important site for O_2 reduction to generate superoxide (12–18). The latter is a precursor of the reactive oxygen species (ROS) that cause damage to DNA and proteins, leading to cellular aging (19–24). The mitochondrial complexes and their ancestral bacterial counterparts share strong sequence and structural similarities at the level of the three catalytic subunits, and they operate through the same mechanism. This allows use of model systems from yeast and the photosynthetic bacteria to be used to explore at a molecular level how evolution has honed the mechanism so as to minimize this deleterious side reaction.

The two catalytic sites of the complex at which the redox reactions of quinones are processed are the sites of action of a wide range of inhibitors that mimic the quinones (25–31). Several of these are finding applications in medicine, based on differential species specificity, and in agronomy based on fungicidal properties, and an environmentally friendly nature (32–36). Elucidation of the mechanism of action of these inhibitors, and the availability of crystallographic structures showing their binding, promise to have wide applications in drug design and in understanding how resistant strains develop.

Over the past half dozen years or so, our understanding of the bc_1 complex has been greatly enhanced by the availability of crystallographic structures (37–48). These now include structures from seven species ranging across the animal, fungal, bacterial, and plant kingdoms, with occupancy of catalytic sites by a growing number of different inhibitors (at least 10 published at the present count), all interpreted against a background of a detailed mechanistic understanding, a sophisticated toolbox of biophysical and biochemical approaches, and the availability of molecular engineering protocols to allow detailed examination of the structure-function interface.

Structural aspects of the field have been extensively reviewed, and an additional essay would be superfluous if it were not for the rapid advancement of our understanding of the mechanistic interface, and the fact that some recent structures throw new light on these physiological aspects.

Overview of Mechanism

The bc_1 complex functions through a Q-cycle mechanism (49–54) (Figure 1). The coupling to proton transfer depends on a bifurcated reaction at the Q_o-site of the complex, in which the two electrons from ubihydroquinone (quinol, QH_2) are passed to two different chains. The initial acceptor of the first electron from quinol is the [2Fe-2S] cluster of the Rieske iron sulfur protein (ISP), which feeds electrons via a bound *c*-type heme [cytochrome (cyt) c_1 in the bc_1 complex] to a mobile electron carrier protein (cyt *c*, or c_2 in bacteria) that then reduces a terminal acceptor (cytochrome oxidase in the mitochondrial chain, an oxidized photochemical reaction center in photosynthetic systems). In most mechanistic models, it is supposed from general principles of quinone chemistry (55) that a semiquinone intermediate is formed at the Q_o-site, although no such species

sensitive to addition of Q_o-site inhibitors has been detected (52, 56). The second electron from quinol is passed to a lower-potential chain containing the low (cyt b_L) and a higher (cyt b_H) potential hemes of cyt *b*. This chain spans the membrane and delivers electrons to a second quinone processing site on the other side, the Q_i-site. At this site, quinone (Q) is reduced to quinol (QH_2) through a two-electron gate (57). Because this reaction requires two electrons, the Q_o-site has to turn over twice, oxidizing two QH_2, releasing four H^+, and delivering two electrons successively to each chain. If the complex starts with a quinone in the site, the first electron at the Q_i-site is stored on a bound semiquinone, which is reduced to QH_2 by the second electron. The two successive one-electron reactions lead to uptake of two H^+ on complete reduction of quinone. For the mitochondrial complex the overall reaction is shown in Equation 1; in α-proteobacteria, cyt *c* is replaced by cyt c_2.

$$QH_2 + 2\text{cyt}\,c^+ + 2H_N^+ \leftrightarrow Q + 2\text{cyt}\,c + 4H_P^+ \qquad 1.$$

Here subscripts N and P denote proton uptake from or release into the protochemically negative and positive aqueous phases, respectively.

The Q-cycle shown in Figure 1 is a generalized representation in the context of the structure of a variant of the Q-cycle that accounts for the ability of the complex to operate as an independent enzyme (58). It was proposed to explain apparent anomalies in the pre-steady-state kinetics of the bc_1 complex in chromatophores from the photosynthetic bacteria *Rhodobacter sphaeroides* and *Rb. capsulatus* (50–54), and of the isolated mitochondrial complexes (59–63). This modified version of Mitchell's original Q-cycle (64) was highly constrained by the set of reactions, by the stoichiometry of components, and by measured physicochemical parameters for rate and equilibrium constants, allowing discrimination from the many alternative models proposed at the time (53).

Although recent crystallographic structures have confirmed the main features expected from the Q-cycle, there were several unexpected findings. The most dramatic finding was the evidence for a large domain movement of the ISP to bring the tethered extrinsic domain containing the [2Fe-2S] cluster to two distinct reaction sites (39, 65–67). At the interface on cytochrome *b* near the Q_o-site (*b*-interface), the ISP oxidizes quinol and then moves through $\sim$25 Å to deliver an electron to cytochrome c_1 (at the *c*-interface), as shown by the four different positions of the [2Fe-2S] cluster (a sample from the many different positions found in different crystals) in Figure 1. Mobility of the ISP extrinsic head has been the subject of much recent work, and the results have provided strong evidence that movement is required for catalysis (3, 68–72). The movement implies participation of five catalytic interfaces in turnover, the three sites (Q_o, Q_i, cyt c_1) expected from the modified Q-cycle model and two more for the catalytic interfaces at which ISP reacts. An important secondary conclusion is that the mobile extrinsic head acts as a second substrate at the Q_o-site (65–67, 73).

QH_2 Oxidation at the Q_o-Site

STRUCTURAL CONSIDERATIONS None of the structures available to date shows any native occupant of the Q_o-site, so our discussions of mechanisms have been based on occupancy by inhibitors and extrapolation by inference to involvement of ligands that interact with them. The site for inhibitor binding is in the cyt *b* subunit, close to heme b_L. The site is spacious, reflecting the differential binding of inhibitors in two main domains (2, 3, 41, 67) (Figure 2).

Inhibitors of class I, typified by the first example, 5-undecyl-6-hydroxy-4,7-dioxobenzothiazol (UHDBT) (25), bind in a domain distal from heme b_L (the distal domain). These are represented in structures by stigmatellin, HHDBT (the inhibitor has a heptyl instead of the undecyl tail of UHDBT), and 2-nonyl-4-hydroxyquinoline N-oxide (NQNO). They interact with the reduced ISP (ISPH), bound at the *b*-interface, through an H-bond to N_ε of the His-161 imidazole, which also binds one of the Fe-atoms of the cluster through N_δ. This interaction leads to an increase in E_m for ISP and to changes in the EPR spectrum in the g_x band. For stigmatellin, a ring >C=O is the H-bond acceptor from the histidine –NH of the ISPH. A second ligand, from the $-COO^-$ group of Glu-272, binds stigmatellin from cyt *b*, forming an H-bond to an –OH group across the chromone ring from the carbonyl group (43, 67, 73) (see Figure 2). The inhibitor UHDBT was also reported to bind in this domain (41), but coordinate data for the structure are not available. However, a recent high-resolution structure by Palsdottir et al. (45) (PDB 1p84) of the yeast complex with HHDBT bound shows the configuration. Two interesting features of this new structure deserve attention. (*a*) Earlier experiments had suggested that the acid form of the inhibitor UHDBT was active because the titer increased as the pH was raised above the pK at 6.5 (74). However, unexpectedly, the structure shows that the group interacting with His-161 is the –OH rather than one of the >C=O groups, and spectrophotometric data suggest that this is in the dissociated form, which would be necessary for an H-bond acceptor function required for interaction with the reduced ISP, and would be in line with the fact that the pH for crystallization was well above the pK for this group measured at 6.1. (*b*) The second ligand, from Glu-272, is not involved in binding. Instead, the side chain points away from the inhibitor, in a configuration similar to that in native or in myxothiazol-containing structures (39, 67, 73). Other inhibitors showing similar binding behavior to that of UHDBT are 2-hydroxy-1–4-naphthoquinones like UHNQ (26, 75) and atovaquone (9, 33, 46, 76). The latter has been modeled as binding in the Q_o-site in a configuration similar to that for HHDBT (46).

Another recent structure of the bovine complex shows binding of NQNO at the Q_o-site (1nu1) (47). This inhibitor, and the n-heptyl analog HQNO, had generally been regarded as relatively specific reagents for the Q_i-site (27, 77), and the report by Gao et al. (47) studies mainly this interaction. However, the crystals also showed density at the Q_o-site, which was modeled as NQNO binding in a configuration similar to stigmatellin, with the –OH group forming an H-bond with N_ε of His-161

of the ISP, and the –NO group forming a water-mediated H-bond with Glu-271 (equivalent to Glu-272 in chicken or yeast). Both these assignments are problematic since an –OH would not form an H-bond with the $-N_eH$ of the reduced ISP, and the $-N^{\delta+}O^{\delta-}$ group is generally considered to be highly polar in solution and would not be expected to form an H-bond with the carboxylate group. The authors speculate that the structure is tautomeric, with the H-atom shared between HO-(ring)-$N^{\delta+}O^{\delta-}$ and O=(ring)-N-OH forms. The latter form is found in the solid state and would provide more natural partners to the stigmatellin ligands.

The second class of inhibitors (class II), typified by myxothiazol, bind in the domain proximal to heme b_L (proximal domain) and do not interact with the ISP, which, in most structures, is found at the *c*-interface (41, 67). Other inhibitors in this class are MOA-type inhibitors such as MOA-stilbene, mucidin, and strobilurin (28), and also famoxadone, whose pharmacophore forms a similar H-bond (see below) (44). Anomalous features of the famoxadone-containing structure are discussed below. An important characteristic of all these structures was the finding that the Glu-272 side chain was rotated away from the liganding position in the stigmatellin-containing structures.

Both classes of inhibitor access the pocket from the lipid phase through the same relatively constricted tunnel, and, especially for those with hydrophobic tails, their binding volumes overlap substantially in the volume around the tunnel, accounting for the displacement of one class by another (67).

In general, the protein structure accommodates itself to the inhibitors and changes quite substantially, depending on occupancy. A significant factor in this accommodation is the configuration of Glu-272. In the stigmatellin-containing structures (43, 65–67, 73), the side chain occupies a major part of the volume in which the pharmacophore of myxothiazol (and other MOA-type inhibitors) would have to sit in that structure (Figure 2). To accommodate myxothiazol (or the other MOA-inhibitors), the side chain of Glu-272 rotates through at least 120° to a new configuration in which it contacts a water molecule at the end of a chain of H_2O leading to the P-phase water (67, 73), the proximal domain expands, and the distal domain closes up (67, 78). The rotation moves the Glu-272 side chain to allow the pharmacophoric group of each of the proximal domain inhibitors to form an H-bond to the backbone –NH (44, 67), a characteristic configuration for this class.

The structure containing the recently characterized inhibitor famoxadone (79) also shows occupancy of this proximal domain and rotational displacement of Glu-272 (44). As a novel feature, the hydrophobic tail of this inhibitor is on the opposite end of the structure compared with myxothiazol (the tail is attached to the pharmacophoric head), and accommodation of the extra volume distorts the protein further (compared with the distortion with myxothiazol). In a detailed analysis of the structure containing famoxadone, Gao et al. (44) suggested that, in addition to an H-bond to the backbone –NH of Glu-272 that famoxadone has in common with the MOA-stilbene and myxothiazol structures (67), aromatic interactions contribute strongly to the binding forces in this domain. Interestingly, the interaction of the rings of famoxadone with the aromatic side chains of the

protein could be convincingly modeled by superposition of a crystal lattice of benzene (44). In contrast to the other class II inhibitors, the famoxadone-containing structure showed the ISP mobile domain at the *b*-interface. The distance from the His-161 of ISP to the inhibitor was ~6.7 Å, too great to allow any specific liganding. Because occupancy of the *b*-interface could not be attributed to any direct interaction with famoxadone, the authors proposed that indirect forces arising from the structural accommodation were responsible, and they discussed some possible candidates.

MECHANISTIC CONSIDERATIONS Critical features of the modified Q-cycle were the recognition that the complex operated as an independent enzyme (58) and that oxidation of two equivalents of QH_2 at the Q_o-site were necessary for complete turnover of the complex (50, 51). In the presence of antimycin as an inhibitor at the Q_i-site, turnover of the complex was limited because electrons could not leave the *b*-heme chain. Although four oxidizing equivalents, two in each of the chains (ISP_{ox} and cyt c_1^+, hemes b_L and b_H), were available to accept electrons from QH_2, the two QH_2 oxidation reactions had different equilibrium constants. Consumption of the more favorable acceptors on oxidation of the first QH_2 constrained oxidation of the second QH_2 by the low value for the second of these ($K_{eq} \sim 1$) and effectively limited the antimycin-inhibited complex to oxidation of the first QH_2 (53, 54, 80). Furthermore, the first electron entering the oxidized high-potential chain was shared between available acceptors, predominantly ISP_{ox} and ferricyt c_1, with a distribution at pH 7 that favored reduction of ISP_{ox} as the higher-potential component. This fraction was therefore not seen in the kinetics measured at wavelengths appropriate for cyt c_1 and c_2 (cyt c_t). These features appeared to account for the kinetic mismatch between the rates of reduction of cyt c_t and b_H in the absence or presence of antimycin that had previously seemed contrary to the Q-cycle (reviewed in 53). Despite this simple explanation, several authors have recently discussed alternative scenarios in which rate limitation was suggested to occur at a step other than the first electron transfer reaction itself. In the simplest of these schemes, the kinetic disparity between rates of reduction of cyt c_1 and cyt b_H seen in mitochondrial complexes has been taken as evidence for a kinetic impediment at the level of ISP movement (81–83). Several groups have espoused more complex schemes involving conformational gating of electron transfer between the Q_o-site and cyt c_1 through a indirect coupling; the reduced ISP is held in position close to cyt *b* until released by conformational changes linked to electron transfer events elsewhere in the complex. These events have been variously suggested to be the electron transfer from a semiquinone-ISP_{red} complex to heme b_L (84–86), electron transfer in the *b*-heme chain (83), rotation of Glu-272 associated with release of the second proton (87), and events at the Q_i-site (81, 86). Some support for gated mechanisms has come from structures. In several of these, marked asymmetries between the two halves of the dimeric complex have been observed (40, 88), and it has been suggested that these show short- or long-range conformational couplings that might be linked to dissociation of the ISP_{red} (4, 86–90).

The structure from Gao et al. (44) with famoxadone in the Q_o-site showed the ISP locked at the *b*-interface, but without the liganding through His-161 assumed to provide the force for this locking with other inhibitors. Xiao et al. (91) investigated the kinetics of reduction of cyt c_1 by ISPH in the presence of famoxadone. They provided clear evidence for constraint on movement of the ISP mobile domain, based on a slowed electron donation to cyt c_1 in the presence of the inhibitor. In these experiments, the isolated complex from bovine mitochondria or *Rb. sphaeroides* was photoactivated through ionically bound ruthenium complexes. The slowed kinetics were taken as providing support for mechanisms in which the ISP movement was gated. From our own studies with famoxadone on the complex in situ in *Rb. sphaeroides*, this kinetic impediment was not apparent under conditions in which the quinone pool was oxidized or 30% reduced, when famoxadone behaved just like myxothiazol, so that ISPH reduced cyt c_1 more rapidly than in the absence of inhibitor. However, some inhibition was apparent when the pool was completely reduced (D.R.J. Kolling & A.R. Crofts, unpublished); possible explanations for this apparent discrepancy are currently being explored.

We have recently demonstrated that the assumptions used in derivation of the modified Q-cycle are sufficient to account for the data obtained in *Rb. sphaeroides* without the need to invoke alternative explanations based on allosteric control of the movement or dissociation of the mobile extrinsic ISP domain (54). We also showed that all reactions associated with association and dissociation of ISP at binding sites, and movement in either direction, occurred more than an order of magnitude faster ($\tau < 30\ \mu$s) than the limiting reaction, and with low apparent activation barriers ($\sim$20 kJ mol^{-1}) (52, 54, 93, 94). The rate constants measured for the limiting reaction, the rate constant inferred for reduction of cyt c_1, and the activation energy for reduction of cyt c_1, have all been confirmed by direct measurement in the isolated *Rb. sphaeroides* complex (92). Because the simple explanation is sufficient in the case of the well-characterized reactions in *Rb. sphaeroides*, extension of these concepts to the mitochondrial complexes would likely be straightforward and should be explored before more complicated mechanisms are proposed. However, such an extension requires measurement of appropriate physicochemical parameters and the kinetics of all components. The extensive data from de Vries and colleagues (60–62) on the pre-steady-state kinetics of the bovine complex demonstrate many of the features expected from the simple hypothesis, but they were interpreted in the context of a double Q-cycle; more recent data using caged-UQH_2 (81) were interpreted in terms of an impediment to movement of ISP. The data set for the yeast complex are less complete and have also been differently interpreted (86, 87, 95).

FORMATION OF THE ES-COMPLEX AT THE Q_o-SITE The overall reaction for oxidation of QH_2 at the Q_o-site of the oxidized bc_1 complex involves the [2Fe-2S] cluster of ISP_{ox} and heme b_L of cyt *b* as the immediate acceptors.

$$QH_2 + ISP_{ox} + \text{heme}b_L \leftrightarrow Q + ISPH + \text{heme}b_L^- + H^+ \qquad 2.$$

The driving force for this reaction is calculated by summing the driving forces for the two partial electron transfer reactions, $\Delta G^{o'} = -F(E_{m,\,ISP} + E_{m,\,bL}) - 2E_{m,\,Q/QH2}) = -2.9\,kJ\,mol^{-1}$, giving a value of $K_{eq} = 3.2$ at pH 7.0, using $E_{m,\,ISP} =$ 310 mV, $E_{m,\,bL} = -90$ mV, and $E_{m,\,Q/QH2} = 90$ mV. Under normal operation, the forward reaction is favored by removal of the electron from heme b_L by rapid transfer to b_H and the Q_i-site, with a more favorable equilibrium constant (50–54). Under physiological conditions, the equilibrium constants for the low potential chain are modulated by the proton gradient, so that under static head conditions, the complex comes into quasi-equilibrium (51).

A more complete description of the energy landscape requires partitioning of the driving force between a set of partial processes, including binding of substrates, activation barriers, electron and proton transfer reactions, and dissociation of products.

Two substrates contribute to formation of the ES-complex, QH_2 and ISP_{ox}, as shown in Scheme 1 (65–67, 73, 78, 96–99). Based on the structure of the stigmatellin-containing complex and following previous proposals for an involvement of ligands from ISP histidines (85, 100), we suggested that the ES-complex was formed with QH_2 in a position at the distal end similar to that found for stigmatellin (67, 73). A likely configuration would involve an H-bond between the ring –OH of the quinol, and the N_ε of ISP His-161, and between the other –OH and the carboxylate of Glu-272. Because of the difference in pK_a values for QH_2 (pk > 11.5) and the ISP histidine (pK ~ 7.6), the quinol –OH is most likely the H-bond donor, requiring that the acceptor N_ε should be in the dissociated (imidazolate anion) form (95, 96). With this in mind, it is possible to account for the strong dependence on pH of the rate of electron transfer over the pH range below the pK_1 at 7.6 in terms of simple enzyme kinetics; the rate varies with [S] (the dissociated form) and approaches saturation (78, 93, 97, 99).

Scheme 1

$$
\begin{array}{ccccccc}
 & & Eb_L.QH_2 & & & & \\
 & QH_2 \nearrow\swarrow & & \nwarrow\searrow\ ISP^{ox} & & & \\
Eb_L & & Eb_L.QH_2.ISP^{ox} & \leftrightarrows \{ES\}^{\#} & \leftrightarrows Eb_L.QH^{\bullet} + HISP^{red} & \leftrightarrows Eb_L^{-} + Q + HISP^{red} + H^{+} \\
ISP^{ox} \searrow\nwarrow & & \swarrow\nearrow\ QH_2 & & & & \\
 & & Eb_L.ISP^{ox} & & & &
\end{array}
$$

THE BINDING CONSTANTS INVOLVED IN FORMATION OF THE ES-COMPLEX A long history from several labs of work in photosynthetic bacteria has shown that QH_2 is preferentially bound compared with Q on oxidation at the Q_o-site, so that the dependence of rate on E_h is displaced from the E_m of the pool (at ~90 mV) to an apparent E_m ~ 130–140 mV (reviewed in 57), but the molecular basis for this displacement of E_m was not understood. It had previously been observed that the steady-state rate of QH_2 oxidation in mitochondrial complexes showed a pH dependence over the range 5.5–9.5 (101, 102), recently attributed to three dissociable groups (103). The stimulation of electron transfer on raising the pH

over the range 5.0–8 was attributed to the need for deprotonation of a group with a pK in the range 5.5–6.5. The rate of QH_2 oxidation during the first turnover of the site, seen in pre-steady-state kinetic measurements of the reactions in *Rb. sphaeroides* chromatophores, showed a similar stimulation, with an apparent pK of ~6.3 (78, 93, 97, 99). A possible candidate for the dissociable group was His-161 of the ISP, but the pK value measured kinetically was displaced from the pK of 7.6 expected to determine the concentration of the dissociated ISP_{ox} form. A straightforward explanation for both these displacements is that they both reflect the same process, formation of the ES-complex, as shown in Scheme 1. Both equilibria are pulled over by the binding process through mass action; the binding of QH_2 will raise the apparent E_m for the oxidation reaction, and the binding of ISP_{ox} will pull the dissociated form of ISP_{ox} out of solution, giving an apparent shift in the pK (78). When the displacements were expressed as equilibrium constants for the binding processes, both sets of data showed similar values, with $K_{QH2} \approx K_{ISPox} \sim 17 \pm 4$ (78, 134). The similarity of these two values supports our suggestion that both reflect that same phenomenon: the liganding between QH_2 and ISP_{ox} involved in formation of the ES-complex. This depends on recognition that the complementary constants in the binding square (left-hand section of Scheme 1) are both small and of the same magnitude (66, 83). Although the thermodynamic equilibrium constants derived here are dimensionless, it seems appropriate to take the values as reflecting binding constants, following the rationale developed by Shinkarev et al. (118) for treatment of binding constants involving the ISP as a tethered substrate.

If this is the case, then the pH dependence over the range below pK_1 is accounted for by the properties of the ISP without invoking any controlling effect of other dissociable groups (see 103). (The slowing of the rate at pK above 8.0, likely determined by pK_2 of ISP_{ox}, is discussed more extensively below). The configuration of the ES-complex suggested requires specific properties of the histidine side chain involved; it has to be the group responsible for the pK_1 measured from redox titration as a function of pH. This assignment now seems well justified (104–107). The interpretation of a controlling role for this pK in determining the occupancy of the ES-complex is strongly supported by experiments with a mutant strain, Y156W, in which both the pK, and the whole curve for pH dependence, were shifted up by ~1 pH unit (94).

ROLE OF Glu-272 The conformational change of the buried glutamate side chain (Glu-272) discussed above was revealed in structures from Berry's lab (39, 67, 73). In the presence of stigmatellin (2bcc), Glu-272 had rotated 120° away from a position seen in the native complex (1bcc), where it pointed toward heme b_L, to provide a second ligand to the inhibitor through an H-bond to an –OH group across the ring structure from the –C=O involved in interaction with the ISP. Molecular dynamics simulations (98) had predicted a relatively stable water chain leading from the aqueous phase on the cyt *c* side into the protein along the b_L heme edge to the Q_o-pocket. In the native structure, or that with myxothiazol bound (67), the

Glu-272 carboxylate contacted this water chain. We suggested that the two ligands that bind stigmatellin were also involved in formation of the ES-complex and that protonation of the Glu-272 carboxylate after formation of the SQ intermediate, followed by a rotation of the Glu-272 acidic side chain between the two positions, could provide a plausible pathway for transfer of a second proton from the site on oxidation of QH (67, 73). Consistent with this, mutant strains with the equivalent glutamate in *Rb. sphaeroides* (E295) modified to aspartate, glycine or glutamine, showed small increases (two- to threefold) in apparent K_m for QH_2, lowered rates of electron transfer, and resistance to stigmatellin (73). The two features required for this mechanism, orientation of Glu-272 seen in the stigmatellin structure (2bcc) and the water chain we predicted, have now been found in higher resolution structures. One of these is the yeast complex with stigmatellin from Hunte et al. (43, 108), from which these authors reached similar mechanistic conclusions. Both features are also well resolved in a recent 2.1 Å structure of the bovine complex (1pp9) (E.A. Berry, personal communication). The contribution of the H-bond from Glu-295 (Glu-272) to the binding of QH_2 is likely in the range ≤ 1 kJ mol^{-1}, as judged from the small increase in K_m for QH_2 in mutant strains (73). Palsdottir et al. (45) found the orientation of Glu-272 toward the water chain in their HHDBT structure, and Gao et al. (44) in their famoxadone structure. Palsdottir et al. (45) provide an interesting discussion of how secondary ligands might orient the QH_2 substrate in the site so as to provide a favorable configuration for binding to ISP_{ox} on formation of the ES-complex.

THE $g_x = 1.80$ COMPLEX The $g_x = 1.80$ line in the CW X-band EPR spectrum of ISP is observed only when the quinone pool is oxidized and ISP reduced (109), and is attributed to interaction between Q and ISPH. As discussed in greater detail below, this likely involves an H-bond between the quinone –C=O and the N_ε of His-161. Ding et al. (100, 110, 111) suggested a strong binding of a quinone by the ISPH to form the Q_{os} species of their double-occupancy model. However, a weakly bound complex seems to be required by the need for rapid dissociation of ISPH to allow participation in catalysis (65–67, 93). To explore the structure in greater detail, we used pulsed EPR to show that the g_x line position change involved an N-atom ligand to the [2Fe-2S] cluster (tentatively identified as N_δ of the histidine ring of His-161) with structural characteristics (as determined from the spin interaction) similar to those seen in the stigmatellin complex (112). In both the stigmatellin and quinone complexes, the involvement of N_ε in an H-bond with the occupant changed the spin interaction of the N_δ with the cluster in a similar fashion. The ESEEM and HYSCORE ^{14}N spectra of both these bound forms differed from that seen in the presence of myxothiazol, where the liganding histidines are likely exposed to the aqueous phase. This supported the view that a similar H-bond was formed [shown in the stigmatellin structure (39, 65) as between a ring >C=O of the occupant and the $-N_\varepsilon H$ of His-161], and represented the first direct structural information about occupancy of the Q_o-site by a quinone species. The Q.ISPH complex is formally an EP-complex, and the strength of this

bond is therefore a parameter of thermodynamic interest in defining the energy landscape.

THE STRENGTH OF THE BOND INVOLVED IN FORMATION OF THE $g_x = 1.80$ COMPLEX Since the first demonstration in the case of UHDBT binding (25), a substantial literature on the change of E_m of the ISP in the presence of similar inhibitors has been interpreted in terms of a preferential binding of the reduced ISP by the inhibitor (31, 46, 75, 113). This has been challenged in a recent study (114), in which the kinetics of binding were measured by mixing dilute suspensions of inhibitor and isolated complex and then assaying the fraction in the active form by addition of excess substrate (DBH) and measurement of the steady-state turnover. Binding was shown to be second order [first order in (inhibitor)], with time constants in the 10 to 100 s range, depending on the concentrations used. The apparent binding rate constants for stigmatellin and myxothiazol were relatively independent of the redox state of the complex before mixing with inhibitor, and this was interpreted as showing that the binding of stigmatellin to oxidized and reduced ISP was at the same rate, i.e., no preferential binding to the reduced form. An alternative explanation is that the rates measured were limited by the probability of interaction of inhibitor and complex to form a bound micellar state, and that this (second-order) rate was independent of redox status. On reduction of the complex with DBH, the bound inhibitor would find the reduced ISP on the ms timescale, and this kinetic event would be undetected in the steady-state assay of turnover. This interpretation avoids the apparent conflict with the previous strong evidence for binding of stigmatellin or UHDBT to the reduced ISP.

In light of the change in E_m of ISP consequent on the binding of class I inhibitors, the interaction of ISPH with quinone might also be expected to induce an increase in E_m ISP, because the pulsed EPR data had shown that a similar bond is involved (112). Such a change in E_m has been measured directly by redox titration (115, 116) and indirectly by looking at the change in kinetics of cyt *c* on flash activation of chromatophores with and without addition of myxothiazol, over the E_h range around the E_m ISP (117, 118). Quantification of the changes showed that the E_m in the presence of myxothiazol was ~40 mV lower than that in the absence of inhibitor (118). Darrouzet et al. (116) investigated changes in E_m ISP in mutant strains with modified linker regions, and reported that myxothiazol induced a downward shift in the E_m ISP so that all strains showed a similar value. In wild type the shift was ~40 mV, comparable to the value found from our kinetic studies and to that with MOA-stilbene (115). From the structural data, no ligand is formed between myxothiazol and ISPH, rather the extrinsic domain is rotated away from its binding site to expose the histidine ligands to the aqueous phase (41, 67, 83). The E_m measured in the presence of myxothiazol therefore likely reflected the unliganded state, so that the change in E_m induced by addition of inhibitor would be due to loss of the bound state seen in the $g_x = 1.80$ complex. From the E_m change, a binding constant of $K_{ass} \sim 4$ could be calculated, showing that >80% of the ISP_{red} would be bound at $E_{h,7} \sim 200$ mV, where ISP is reduced and the quinone

pool oxidized (118). Treatment of the thermodynamics of the binding reactions for the ISP required development of a new formalism appropriate to the peculiar status of the ISP as a tethered substrate (118).

The binding constant for formation of the $g_x = 1.80$ complex ($K_{ass} \sim 4$) is in the same range as that for the binding of QH_2 by Glu-272, as seen in the increased K_m in a mutant strain with glycine instead of glutamate [$K_m^G/K_m^E = 2.4$ (73)], and, following the arguments of Crofts et al. (66), explains why the apparent E_m for formation of the complex titrates with the same midpoint as the quinone pool (110).

IDENTIFICATION OF THE RATE-LIMITING STEP From the above discussion, it seems likely that electron transfer from QH_2 to ISP_{ox} occurs through the H-bond by which the ES-complex is stabilized, and that it involves the dissociated ISP_{ox}. Because the pK on the reduced ISP is >12 (107), electron transfer is coupled to H^+ transfer and the reaction is formally an H-transfer. Release of the proton occurs on oxidation of ISPH by cyt c_1 (above pK_1) or on rebinding of $ISP_{ox}H$ in the ES-complex (below pK_1).

Previously, Brandt & Okun (102), using a steady-state assay, confirmed the pH dependence for the steady-state rate of oxidation of ubiquinol by isolated bovine bc_1 complex observed by Link & von Jagow (101), and extended these studies to plastoquinol analogues and the yeast bc_1 complex. They also reported a novel dependence on pH of the activation energy for the steady-state turnover. From the pH dependence of the rate, they identified two controlling groups, one with a pK at 6.5 and a second at 9.5. The former group had to be in the dissociated state, and the latter protonated for rapid electron transfer, accounting for the bell-shaped pH dependence. Because of the pK values, they excluded any involvement of the ISP histidine group with its pK_1 at 7.6. On the other hand, the pH dependence of the activation energy was interpreted as showing that deprotonation of QH_2 was a necessary intermediate step preceding electron transfer. This followed earlier work by Rich & Bendall (172) on the non-enzymic oxidation of quinol by cyt *c*, which showed a strong acceleration of rate in the high pH range. This was interpreted in terms of a reaction mechanism dependent on QH^-, with the low probability of deprotonation providing the activation barrier. In contrast, the bc_1 complex catalyzed reaction showed a rate that decreased dramatically in this range. Because of this contradictory result, the mechanistic speculations had to be based on the pH dependence of the activation energy. Brandt & Okun (102) suggested that, following binding of the neutral quinol to the catalytic site, deprotonation to the quinol anion with direct release of the proton to the aqueous phase, with a pK in the range 14–16, was necessary before electron transfer could occur, and that this was responsible for most of the activation barrier. The deprotonation of QH_2 was incorporated into a detailed reaction scheme, the "proton-gated charge transfer mechanism," which included a double-occupancy model for electron transfer to heme b_L and control of the overall reaction by the redox state of heme b_L.

The earlier studies of Crofts & Wang (52), on the pre-steady-state kinetics of the complex in its native state in *Rb. sphaeroides*, and more recent extensions of

this work by Hong et al. (93) have shown the following:

1. The reaction with the slowest rate under conditions of substrate saturation was the oxidation of QH_2 at the Q_o-site (52). This was also the reaction with the highest activation barrier (52, 93).
2. The rate of QH_2 oxidation showed the same bell-shaped pH dependence as seen in mitochondrial complexes, as discussed above (93, 94).
3. In contrast to the results of Brandt & Okun (102), the activation barrier was independent of pH (52, 93). Since varying pH below the pK_1 for ISP_{ox} varies the concentration of the dissociated ISP_{ox} species that is active in formation of the ES-complex, the activation barrier was independent of concentration for this substrate (93).
4. The activation barrier was also independent of the redox poise of the quinone pool (52, 93). Since reduction of the quinone pool increases the concentration of QH_2, the other substrate, these characteristics showed that the activation barrier was independent of substrate concentration, and therefore after formation of the ES-complex, as expected for an enzyme reaction.
5. The limiting reaction was transfer of the first electron from QH_2 to ISP_{ox} (93, 94).

These data were clearly at variance with those of Brandt & Okun (102) and precluded a mechanism of the sort they suggested. As shown by the pH dependence of the rate, and the acceleration of rate on reduction of the pool, the rate varied with concentration of either substrate, as expected from simple Michaelis-Menten considerations. The movement of the ISP could be assayed by measuring the lag times involved in reactions that incorporate it as a partial process. The time not accounted for by electron transfer events was always short (<30 μs), and the reactions had low activation barriers (54, 93). This was in line with weak association constants and the simple constrained diffusion mechanism suggested by the structures (65) and a steered MD simulation (98).

DEPENDENCE OF RATE ON DRIVING FORCE AND ON pH Analysis of the kinetics in strains with mutations in ISP that lowered the E_m value had shown that the rate of QH_2 oxidation by the isolated complex depended on the driving force for the first electron transfer (119–121). We showed a similar dependence on driving force in pre-steady-state measurements assaying oxidation of the first QH_2 for the complex in situ (93, 94, 122). Similar mutations made in *Rb. sphaeroides* (94), *Paracoccus nitrificans* (121), and in yeast (120) all showed the same behavior. In contrast, the overall rate did not show changes consistent with a dependence on driving force on change in E_m of heme b_L (93). Mutant strains showed either a slowed electron transfer with increased driving force or no effect (123–125). The rate of reduction of heme b_L in the presence of antimycin after prior reduction of heme b_H showed the same rate constant and activation energy as the reduction of heme b_H when the latter was oxidized before flash activation (80, 93), although

the redox potential of heme b_L is likely changed through coulombic interaction by ~ -60 mV on reduction of heme b_H to give the $E_m \sim -90$ mV value measured through redox titration (123, 126). This strongly suggested that transfer of the first electron (from QH_2 to ISP_{ox}) was the rate-limiting step, and that of the second electron is intrinsically more rapid. The rate of the second electron transfer is gated [using the definition of Davidson (127); see Scheme 2] by the limiting rate of the first electron transfer. As a result, the change in rate expected on change of driving force is not seen experimentally.

Scheme 2

Definitions of *gated* and *coupled* electron transfer in terms of electron transfer reactions showing kinetic complexity. Adapted from Davidson (127)

Simple kinetic model

$$A_{ox} + B_{red} \overset{K_d}{\Leftrightarrow} A_{ox} \cdots B_{red} \underset{-k_{lim}}{\overset{k_{lim}}{\Leftrightarrow}} A_{red} \cdots B_{ox}$$

Kinetic complexity

$$A_{ox} + B_{red} \overset{K_d}{\Leftrightarrow} A_{ox} \cdots B_{red} \underset{-k_x}{\overset{k_x}{\Leftrightarrow}} [A_{ox} \cdots B_{red}]^{\#} \underset{-k_{ET}}{\overset{k_{ET}}{\Leftrightarrow}} A_{red} \cdots B_{ox}$$

For true ET

$k_{ET} << k_x$ $\quad K_x\,(k_x/k_{-x}) >> 1$ $\quad k_{lim} = k_{ET}$ $\quad \lambda_{obs} = \lambda_{et}$

For ***gated*** ET

$k_x << k_{ET}$ $\quad k_{lim} = k_x$ $\quad \lambda_{obs} = f(\Delta G^{\#}_x)$

For ***coupled*** ET

$k_{ET} << k_x$ $\quad K_x\,(k_x/k_{-x}) << 1$ $\quad k_{lim} = K_x\,k_{ET}$ $\quad \lambda_{obs} = f(\lambda_{ET}, \lambda_x)$

What controls the rate of the first electron transfer? The structures, and our speculation on the nature of the ES-complex, provided an opportunity to analyze the rate in the context of the distance for electron transfer (93). In the context of the proposed structure of the ES-complex, the rate of the first electron transfer was slower by about three orders of magnitude than that expected from the distance of $\sim$7 Å suggested by our model (73, 93) and considerations by Moser et al. (128). The problem then was to account for this slow rate. The observed rate could be explained if a high value for reorganization energy ($\lambda \sim 2.0$ eV) was used, in line with the high activation barrier (93), but this value was much higher than that found in other electron transfer reactions occurring over similar distances (128), and no explanation was obvious from the structure.

PROTON-COUPLED ELECTRON TRANSFER AS A MODEL FOR QH_2 OXIDATION AT THE Q_o-SITE Work on proton-coupled electron transfer in model compounds by

Nocera and colleagues (129) has emphasized the controlling effect of relative pK values on H^+ transfer through H-bonds. A detailed theoretical treatment by Cukier & Nocera (130) discussed the control of rate in terms of a Marcus treatment of proton-coupled electron transfer. Paddock and colleagues (131), in discussion of the proton-coupled electron transfer reaction at the Q_B-site in photochemical reaction centers, made simplifying assumptions that allowed separation of the role of the proton transfer from the electron transfer, by treating the former through a probability function. Combining these approaches led us to propose a treatment of the dependence of rate on driving force as applied to the Q_o-site reaction (99, 134), which avoids the difficulties arising from quantum mechanical considerations of the role of the proton (130).

(*a*) The electron transfer can occur only when the proton configuration is favorable. This requires that the proton be transferred through the H-bond before electron transfer can occur.

$$\mathrm{E}\cdot b_\mathrm{L}\cdot \mathrm{QH_2}\cdot \mathrm{ISP_{ox}} \overset{\Delta G_{proton}}{\leftrightarrow} \mathrm{E}\cdot b_\mathrm{L}\cdot \mathrm{QH^-}\cdot \mathrm{H^+ISP_{ox}}$$

$$\overset{\Delta G^{\#}_{electron}}{\leftrightarrow} \mathrm{ES^{\#}} \rightarrow \mathrm{E}\cdot b_\mathrm{L}\cdot \mathrm{QH^{\bullet}}\cdot \mathrm{ISPH}. \qquad 3.$$

$$\Delta \mathrm{G_{proton}} = -2.303\,\mathrm{RT}\left(\mathrm{pK_{ISPox}} - \mathrm{pK_{QH_2}}\right). \qquad 4.$$

(*b*) The occupancy of the proton-transfer state needed for electron transfer is determined by the pK values of the H-bond donor and acceptor through a Brønsted term, ΔG_{proton}. Given the pK values for QH_2 ($pK > 11.5$) and ISP_{ox} ($pK \sim 7.6$), the configuration is thermodynamically highly unfavorable, and the low probability of accessing the state represents a substantial part of the activation barrier. The step represented by $\{ES\}^{\#}$ in Scheme 1 is replaced by the two partial processes shown in Equation 3.

(*c*) Rates of H^+ transfer through H-bonds are inherently rapid ($\sim 2.10^{11}\ s^{-1}$) (132, 133), ~1000 faster than the maximal electron transfer rate at this distance. To a good approximation, the proton transfer contribution can therefore be treated as a separate probability function given by the Brønsted term. This treatment corresponds to the limit condition of a coupled reaction (127; see Scheme 2). In terms of reaction rate theory, this is equivalent to partitioning the activation barrier into the sum of terms, ΔG_{proton} and $\Delta G^{\#}_{electron}$ in this case, which can then be split out into separate terms in the Arrhenius equation and its derivatives. This allows for a great simplification in thermodynamic treatment. Using the pre-exponential terms suggested by Moser et al. (128), the following equation for the rate constant was proposed (99, 134):

$$\log_{10} k = 13 - \frac{\beta}{2.303}(R - 3.6) - \gamma\frac{\left(\Delta G^{o}_{ET} + \lambda_{ET}\right)^2}{\lambda_{ET}} - \left(pK_{QH_2} - pK_{ISP_{ox}}\right). \qquad 5.$$

Here β is 1.4, the slope of the Moser-Dutton relationship between $\log_{10}k$ and distance, R is the distance in Å, ΔG^o_{ET} is the driving force for the electron transfer step, and λ_{ET} is the reorganization energy (both in V). The factor γ in the above equation has a value of ~3.1 in the Moser-Dutton treatment, which differs from the value of 4.227 at 298 K ($\gamma = F/(4 \times 2.303\ RT)$ from classical Marcus treatment by incorporation of quantum mechanical factors contributing to a tunneling component (135–137).

The explanation involving the pK of QH_2 as a determinant in the activation barrier recalls the earlier suggestions that deprotonation of QH_2 might provide the activation barrier (102, 172). However, the reaction here is not a deprotonation, but formation of an improbable intermediate state. The electron transfer through the H-bond is coupled to proton transfer, and this provides a direct explanation for the pH independence of the activation barrier. The reaction mechanism proposed is well justified by theory and experiment (134). In contrast to the previous proposal (102), a substantial barrier to the electron transfer step is also necessary to explain the dependence on redox driving force demonstrated in mutant strains.

THE ODD BEHAVIOR OF STRAIN Y156W Our own work on the dependence of reaction rate on driving force used mutant strains with modifications in ISP at Tyr-156 (Tyr-165 in bovine sequence), which forms an H-bond from the –OH to the Sγ of one of the cysteine ligands (Cys-139, bovine) (94). Measurement of the E_m and pK values of these strains showed decreases in E_m for all, but one strain (Y156W) also showed a substantial increase in pK (from 7.6 to 8.5). When $\log_{10}k$ for oxidation of QH_2 was plotted as a function of ΔE_m at pH 7.0, the points followed the dependence of rate on driving force expected from Marcus theory (135–137). However, a substantial part of the inhibition observed in strain Y156W could be attributed to the effect of the pK change on the concentration of the dissociated form as substrate; if this contribution was considered, the data point for this strain no longer fell on the same curve as those for other mutants. This anomaly might have called into question the validity of using the Marcus explanation for the inhibitory effect observed (94), but can now be explained by consideration of the role of pK_1 of ISP_{ox} in controlling several critical parameters:

1. In the formation of the ES-complex, the dissociated (imidazolate) form is the substrate (see above). The concentration of this form depends on pH and on pK, assumed to be pK_1 due to dissociation of His-161, leading to the dependence of rate on pH over the range 5.5–8 in wild type.
2. The pK_1 at 7.6 on the oxidized form also results in a dependence of $E_{m,\,ISP}$ on pH, the value decreases above pH 7.0, with a ~59 mV/pH unit slope above the pK. Over this range (at pH > 8), the overall rate and the rate of the first electron transfer both decrease. The decrease in E_m of ISP above pK_1 might be expected to determine the overall driving force, but because the E_m of the Q/QH_2 couple also decreases by ~59 mV/pH, the driving force is constant with pH over the range of pK_1. A second pK (pK_2) on the oxidized form at

~9.6 increases the slope of pH dependence at higher pH. As a consequence, pK_2 will be the critical determinant for the change in driving force; the fall-off in rate over the high pH range can be attributed to the loss of driving force as the effect of pK_2 comes into play.

3. The pK_1 also plays a critical role in determining the activation barrier through the Brønsted term discussed above. From Equation 5, an increase in pK_1 should lead to a lowering of the Brønsted barrier, and hence in increase in rate.

The curves showing the dependence of rate on driving force using mutant strains could be well fitted by using Equation 5 above (134). In particular, the anomalous behavior of strain Y156W with a shifted pK could be explained by recognizing that two effects of the pK_1 value offset each other. The lowered rate due to the substrate effect (depletion of the dissociated ISP_{ox} at $pH < pK_1$, as in 1, above) was compensated by an increased rate constant associated with a lower activation barrier, due to the smaller contribution of the Brønsted term (as in 3). This simple explanation of the odd behavior provides strong support for the mechanism proposed.

The equilibrium constant between cyt c_1 and ISP is also determined by E_m ISP, because E_m cyt c_1 is independent of pH. This has important consequences in the kinetics of the high-potential chain measured in pre-steady-state experiments (92, 139) and can also be used to vary the driving force, so as to favor the forward electron transfer at higher pH. Engstrom et al. (92) used this effect, as well as mutant strains with modified $E_{m,ISP}$, to investigate the Marcus relationship for this reaction and found a rate independent of driving force. Since the observed rate was much slower than that calculated from the closest configuration suggested by the structures, they concluded that the reduction of cyt c_1 by ISPH was gated (127) by a conformational transition from a nonreactive state. From the high rate constant and the low activation barrier observed, this was a process different from the rate-limiting QH_2 oxidation reaction.

TRANSFER OF THE SECOND ELECTRON AT THE Q_o-SITE It has long been recognized that the semiquinone intermediate formed after the first electron transfer has the potential for reduction of O_2, thus providing an explanation for the generation of superoxide observed at this site in mitochondria (12–15). This provides a background to discussion of the second electron transfer through which this potential hazard is minimized; the SQ is removed by rapid oxidation through the b_L heme. Evolution has honed the mechanism to limit the damage; the overall rate has to be optimized while keeping the species that reacts with O_2 at a minimal concentration and/or limiting access of the intermediate to O_2.

Hong et al. (93) discussed mechanisms for the second electron transfer, from SQ to heme b_L, that were compatible with the kinetic and thermodynamic properties, measured activation barriers, and structural information. They noted that the product of rate constant and fractional occupancy of the SQ intermediate state

would be critical in determining the rate. The rate constant was determined by the distance to heme b_L and substitution of appropriate values into the equation of Moser et al. (128). Occupancy was determined in a complicated fashion by the parameters of the first electron transfer through the relation between E_m, driving force and semiquinone stability. Because the overall rate appeared to be determined by transfer of the first electron and was independent of the driving force for the second electron transfer, the gating of the latter by the former implied an intrinsic rate much faster than the rate-determining step. From these considerations, Hong et al. (93) ruled out single-occupancy mechanisms in which the occupancy of the intermediate state was very low and the intermediate was constrained to the distal domain. On the basis of these criteria, several sorts of hypothesis seem plausible:

1. Link (84) suggested that the product of the first electron transfer might be a complex between SQ and the reduced ISP in which a strong binding constant prevented oxidation of ISPH by raising the E_m value above that of the acceptor. Crofts and colleagues (67, 73, 93), with the benefit of the structural information by then available, have considered a modified version of this hypothesis, in which the strong binding constant prevented dissociation to products until after the second electron transfer from SQ to heme b_L. The intermediate complex would bind up the semiquinone, so that it was not available to O_2, and also bind up the ISPH, to prevent its movement, and oxidation down the high potential chain that would allow the ISP_{ox} to grab the second electron from the semiquinone and bypass the bifurcation. In this intermediate complex, the SQ could be relatively stable and therefore at high-enough occupancy to allow electron transfer at the observed rate from the distal domain in which the complex would have to be formed. Because neither SQ nor ISPH has been detected by EPR under conditions in which this complex might be favored (52, 56), it was necessary to introduce an additional ad hoc hypothesis, that both EPR signals were quenched through mutual magnetic interaction (56, 84). As Palsdottir et al. (45) noted, their recent structure of the complex containing HHDBT might be considered as mimicking an intermediate state in which the SQ is in the anionic form, complexed with the reduced ISP, after transfer out of second H^+ and before dissociation of the $SQ^- \cdot$ ISPH state. If this analogy is correct, their structure gives support for the Link (84) model. However, the stability of the inhibitor-ISPH complex might not necessarily reflect the stability of the $SQ^- \cdot$ ISPH complex. Since the side chain of Glu-272 is rotated away from liganding configuration in their structure, it might more conservatively be seen as providing support for the role of this residue in proton transfer.
2. An alternative mechanism was proposed by Crofts and colleagues (52, 67, 73, 93) in which the SQ was formed at very low concentration (thus minimizing reaction with O_2), owing to an unfavorable equilibrium constant. To overcome the kinetic barrier arising from the low occupancy suggested by the data, the semiquinone would have to move within the site closer to

heme b_L. From the distance obtained by modeling a quinone in the proximal domain to replace myxothiazol, the closer approach would provide a rate constant ~1000 times more rapid than from the distal domain. The movement proposed would require dissociation of the intermediate product complex before electron transfer to heme b_L could occur. On dissociation of the SQ.ISPH complex, the second H^+ would be transferred to the Glu-272 carboxylate, followed by a rotational displacement of the Glu-272 side chain to allow removal of the second H^+ from the site, and to open up the volume of the proximal domain for the $SQ \cdot^-$ (73). Earlier versions of this mechanism were based on the failure to detect either SQ or reduced ISP under conditions in which an intermediate complex would be maximal (52), so this experimental observation was naturally accounted for. The mechanism also accounted naturally for the large volume of the site, and explained the evidence from mutational studies showing that modifications that led to myxothiazol resistance also led to inhibition of electron transfer (67). If the resistance was interpreted in terms of an impediment to binding, then these mutations would also impede binding of SQ in this domain. The inhibition observed seemed to provide a clear indication that occupancy of the proximal domain during catalysis was important. Support for a dissociation of the SQ.ISPH intermediate has come from analysis of bypass reactions at the Q_o-site in the presence of myxothiazol (140, 141). To explain these, Muller et al. (141) interpreted their data as showing that dissociation of SQ.ISPH intermediate must occur, although under these circumstances, electron transfer to heme b_L was blocked (see more extensive discussion, below).

3. A third type of mechanism involves occupancy of the site by two quinones during catalysis, one tightly bound, the other readily dissociable as a substrate (85, 100, 110). The large volume of the site shown by the structures (39, 41, 67), the malleability of conformation suggested by differences in structures with different inhibitors in situ (39, 67, 78), the demonstration of a displacement of two quinones from the complex on binding either of the two classes of Q_o-site inhibitors (142), and different g_x line positions in the EPR spectrum of ISPH on partial extraction of ubiquinone [interpreted as reflecting two different quinone species (100, 110, 111, 115), both lost on addition of either class of inhibitors (100)], all favor double occupancy. Occupancy of the distal domain in the presence of proximal domain inhibitors (2, 111, 115) and the observation that some superoxide can be generated at the site in the presence of myxothiazol or other MOA-type inhibitors (100, 110, 143) demonstrate that occupancy of the two domains is not necessarily exclusive. However, there are major problems in understanding how such a double occupancy of quinone and proximal domain inhibitor might translate to a mechanism for normal turnover (2, 67, 144). Attempts to fit two quinones in existing structures lead to considerable distortion (142; A.R. Crofts, unpublished), and although a structural model has been presented (142), no evaluation of the energetic consequences was reported. The question of

energetic consequences is of importance, because, if this mechanism is to be accepted, double occupancy has to represent a favorable configuration compared to single occupancy. There remains the difficulty of explaining away the failure to find in any of the structures the tightly bound quinone expected (39, 41, 67). In the *Rb. sphaeroides* system, support for double occupancy was based on distinct EPR lines attributed to interaction of ISPH with weakly (Q_{ow}) and strongly (Q_{os}) binding species, or an empty site (100, 110), and the Q_{ow} species was predicted to have a binding constant substantially greater than those for the Q_B site of RC, or the Q_i-site, at both of which structurally well-defined quinones have been characterized. However, in the mitochondrial complexes where the structures show no occupancy, the changes in EPR spectra on extraction could be fit without invoking the additional spectral form associated with Q_{os} (P.R. Rich, personal communication); this could be interpreted as showing that there are substantial differences in binding between the bacterial and mitochondrial systems. Some features of earlier models need revision. The assignment of the quinone interacting with ISP as the tightly binding species (110, 115) must clearly be revised (67), because the ISP mobile domain has to be able to move. Double occupancy would provide an obvious explanation for the evidence indicating that occupancy of the proximal domain is important. However, this introduces a further problem. The differential effects of mutations on inhibitor binding were not reflected in differential effects on the EPR signals interpreted as showing two quinone species, although these would clearly have to be occupying the domains from which the inhibitors are selectively excluded (67, 144). These difficulties have so far precluded more general acceptance of this hypothesis.

4. As noted above, Crofts & Wang (52) considered mechanisms in which the SQ intermediate in the Q_o-site reaction was generated at low concentration, to give an up-hill reaction for the first electron transfer. Constraints on possible values for the equilibrium constant came from the detection limit of the SQ, and from the activation barrier. The former was based on unpublished experiments which showed that no myxothiazol-sensitive SQ could be detected under the "oxidant-induced reduction" conditions (145) expected to maximize [SQ] (K.A. Andrews, R.B. Gennis & A.R. Crofts, unpublished; see 146), leading to a maximal value for $K_{eq} \sim 10^{-4}$. Similar experiments in a mitochondrial complex yielded similar results, with a similar kinetic interpretation (56). The activation barrier represents the limiting value for instability of any intermediate state, giving a minimal value for K_{eq} determined by E^{act}. This lowest limit on K_{eq} represented a mechanism in which both electron transfers could occur simultaneously, with a common activation barrier and an activated state represented by the SQ intermediate; Crofts & Wang (52) discussed this as the most economical hypothesis. Two sets of data have since made this hypothesis untenable: (*a*) Hong et al. (93) and Guergova-Kuras et al. (94) pointed out that the slope of the curve of $\log_{10} k_{cat}$ v. driving force, obtained from experiments in which the driving force was

varied by using mutant strains in which the E_m of ISP was changed, was less steep ($\sim$0.009 mV^{-1}) than the value expected from this minimal hypothesis ($\sim$0.017 mV^{-1}), and therefore excluded such a mechanism; (*b*) Hong et al. (93) considered the constraints of occupancy and distance on rate for the single-occupancy case and concluded that if the rate constant was determined by the distance from a SQ occupant modeled in the distal pocket to heme b_L, the maximal rate possible, given the very low occupancy of the activated state from which the second electron would have to be transferred, would be too slow by several orders of magnitude to allow such a mechanism.

A concerted mechanism involving simultaneous transfer of two electrons to the two separate chains has recently been revisited by Kim et al. (41) and Trumpower and colleagues (3, 87), although they did not comment on the critical points discussed above. To overcome these arguments in the context of a single-occupancy model, it would be necessary to propose that the substrate QH_2 delivers both electrons simultaneously from a state bound in the distal domain with much higher occupancy than the activated state, through pathways that, although very different in terms of the distance involved, local structure, and reaction path, must function to give the same activation barrier and rate constant. A more detailed consideration must await justification of the physicochemical underpinnings of such a mechanism. Any alternative simultaneous model would require a faster rate constant than suggested by the distance. This could perhaps be achieved in a double-occupancy version of this type of mechanism, in which electron transfer was facilitated by a quinone species in the proximal domain. However, it would seem difficult in this context to account for the pattern of dependence on driving force discussed above, which had seemed to demonstrate control through the first electron transfer.

Some discrimination between single- and double-occupancy models might be made on the basis of the role of Glu-272 in liganding of QH_2 and in proton transfer out of the site. If Glu-272 is a ligand in the ES-complex, the volume occupied by the side chain and associated waters would largely fill the volume into which any second quinone would be likely to bind (Figure 2). Because the QH_2 in the distal domain has to be the substrate, there is no room for the strongly bound quinone in this proximal position without substantial distortion. As there is no evidence for any alternative binding domain close enough to heme b_L, this would argue against double-occupancy models being of mechanistic importance. If the glutamate does not serve this function, and a high degree of elasticity of structure without an energetic penalty is demonstrable, a wider set of possibilities remains open.

Discrimination between the first two models is more difficult. The question could clearly be resolved in favor of model 1 if the SQ.ISPH intermediate could be demonstrated by another spectroscopic approach than EPR. With a limiting first electron transfer and low occupancy of the SQ.ISPH state, it would be difficult to discriminate on the basis of the kinetics of reduction of heme b_H. However, the lag phase in the kinetics allows us to put limits on the population of intermediate states. In chromatophores poised with the quinone pool partly reduced, reduction of heme

b_H occurs after a lag of 120 μs. Of this, $\sim$100 μs is accounted for by identified electron transfer events (54). The unaccounted $\sim$20 μs would have to include the times for electron transfer through ISP to the Q_o-site (including movement), and the electron transfer through heme b_L. If the first electron transfer is rate determining, any accumulation of intermediate states (including centers in the SQ.ISPH state) would occur at the rate limit of $\sim$600 μs, at the expense of electrons delivered through heme b_L to b_H. Since no delay of this magnitude is seen, occupancy of any such state must be quite small. When heme b_H is reduced, the reduction of heme b_L follows similar kinetics (80, 93). Since the overall equilibrium constant under these latter conditions is close to 1, any significant stability of the intermediate state would represent an energy trough, but no kinetics that could be attributed to filling of such a trough are detected.

Hong et al. (93) discussed at length the interplay between SQ occupancy and rate for the second electron transfer. A value for $K_{eq} < 0.01$ for the first electron transfer, which seems a reasonable limit based on the lag, would be on the borderline of possible values compatible with electron transfer from the distal domain. A detailed kinetic model would allow exploration of the constraints on occupancy of intermediate states, but none is yet available. More detailed kinetic data, alternative spectroscopies for assaying ISPH [for example, by CD (96, 104)], SQ (by UV/VIS), and the Glu-272 changes (using FTIR), and better-defined models for cases 3 and 4, are needed before a definitive choice can be made between any of the above mechanisms. A computer model to allow exploration of the parameters determining Marcus theory constraints on the rates for the two electron transfers of the bifurcated reaction is available (http://www.life.uiuc.edu/crofts/Marcus_Bronsted/).

ELECTRON TRANSFER FROM CYT C_1 TO CYT C Berry's group had an early report of a bovine bc_1 complex dimer cocrystallized with cyt *c*, showing a weak occupancy of the latter, and an unresolved interaction domain (2; E.A. Berry, personal communication). Among recent structures, Lange et al. (88) have reported a complex between the yeast bc_1 complex and yeast cyt *c* at higher resolution that shows the interaction between cyt c_1 and its electron acceptor. Interestingly, only one of the two monomers had a cyt *c* attached, and asymmetry was also apparent elsewhere in the dimer, especially at the Q_i-site, where the occupancy by quinone was quite different in the two monomers. The authors speculated that these asymmetries were linked and might be of importance in allosteric control. From a mechanistic perspective, the structure shows the interface through which electron transfer between cyt c_1 and cyt *c* occurs, and Hunte et al. (147) presented a detailed analysis of possible electron transfer mechanisms in the light of the structure. The kinetics of electron transfer, the role of particular residues at the interaction interface, and the kinetic changes on mutation at the interface have been explored in detail using photoactivation of a yeast cytochrome *c* derivative labeled with ruthenium trisbipyridine at Lys-72 (148). The authors targeted acidic residues of the interface on cyt c_1 for mutation and concluded that acidic residues on opposite sides of the heme crevice of cyt c_1 are involved in binding with the positively charged cyt *c*,

and that they direct the diffusion and binding of cyt *c* from the aqueous phase between the outer and inner mitochondrial membranes.

MECHANISTIC INFORMATION OF MEDICAL OR PHYSIOLOGICAL INTEREST Detailed analysis of the structural basis of inhibitor function, and the mechanistic information available from mapping of mutations that affect binding to catalytic interfaces, are beyond the scope of this review, but have been discussed extensively elsewhere (1, 2, 8, 9, 41, 44–47, 65–67). Some more recent observations deserve further comment. New structures showing the binding configuration of HHDBT (45), NQNO (47), and famoxadone (44) have been mentioned above. The HHDBT structure has been used to model a likely configuration for the drug atovaquone (46), which is clinically important as an antimalarial agent, based on susceptibility to inhibition at the Q_o-site in *Plasmodium* species [also *Pneumocystis carinii* (pneumonia), *Toxoplasma gondii* (toxoplasmosis), and other fungal parasites] and resistance in vertebrates. The molecular basis for this susceptibility is revealed by mutant strains of *P. falciparum* and other *Plasmodium* species that develop resistance to atovaquone (33; reviewed in 9). Kessl et al. (46) modeled one of these mutations in yeast (L275F) and demonstrated substantial resistance, which was explained in terms of the increased volume of the Phe compared with Leu, which impinged on the binding volume. Figure 3 shows the position in the structure of residues at which resistant mutations are found in relation to the stigmatellin-binding volume.

BYPASS REACTIONS AT THE Q_o-SITE IN THE PRESENCE AND ABSENCE OF OXYGEN As noted above, the well-studied reaction of the Q_o-site with O_2 to produce superoxide (SO) is generally attributed to one-electron reduction by the intermediate semiquinone species generated at the site when transfer of the second electron to the low potential chain is blocked (for recent reviews, see 14, 15). SO production occurs when electrons back up in the low-potential chain so that electron transfer from the intermediate SQ to heme b_L becomes limited. Under physiological conditions, this happens on development of a large back-pressure from Δp and in the lab when antimycin inhibits exit of electrons from the *b*-heme chain. The maximal rate of SO generation is $\sim$2% of the normal turnover.

Several recent reports provide new insights as to the nature of the reaction. In mitochondrial complexes, myxothiazol inhibits the SO production in the presence of antimycin, but only by about 70%. In the absence of antimycin, production of SO is stimulated by addition of myxothiazol to give a similar rate ($\sim$0.6% full turnover) (140, 141). Several groups have argued convincingly that the semiquinone at the Q_o-site is the reductant for O_2 (13–18). Because formation of semiquinone depends on oxidation of quinol, this could occur only if an ES-complex of some sort is formed in the presence of myxothiazol, with occupation of the distal domain of the site by ubiquinol and reaction with ISP_{ox} as the most likely configuration. Since most data seemed to indicate that myxothiazol eliminates all quinone species from the site (67, 100, 142), the possibility of such a double occupancy was surprising.

Muller et al. (141) found that the rate of the bypass reaction was not dependent on the presence of O_2. When the rate of quinol oxidation was assayed by reduction of cyt *c*, the bypass rates observed under anaerobic conditions in the presence of either antimycin or myxothiazol were the same as under aerobic conditions. This could be explained if generation of semiquinone under all conditions was rate-limiting, and independent of $[O_2]$, and if two pathways competed for the semiquinone, both with much higher rate constant, one to O_2 and the other indirectly to cyt *c*. Under aerobic conditions, O_2 out-competes the alternative pathway as acceptor for the second electron. A plausible pathway for the bypass under anaerobic conditions would be via the returning ISP_{ox}, which could oxidize the semiquinone after it had donated the first electron to cyt *c* via cyt c_1. Because the distance from the [2Fe-2S] cluster in the ISP_B position to cyt c_1 would preclude direct transfer from the complexed state (39), the reaction could occur only if the intermediate SQ.ISPH state dissociated to products. The bypass reaction therefore demonstrates that the SQ.ISPH state is not so tightly bonded as to preclude dissociation. A third observation of interest was that increasing the $[O_2]$ fivefold above ambient had no effect on the rate of SO generation in the presence of myxothiazol, but stimulated the rate in the presence of antimycin by ~25% (141). The saturation at ambient O_2 in the presence of myxothiazol indicates a high affinity compared with that in the absence of myxothiazol and shows that at least a fraction of the semiquinone was in a less reactive configuration when the Q_o-site was free of any proximal domain inhibitor (117).

The relation between occupancy of the distal domain and the size of the proximal domain inhibitor has been further explored by Muller et al. (143). They studied the K_m and V_{max} for ubiquinol substrates and showed that, whereas the V_{max} was independent of the nature of the inhibitor, the K_m was markedly dependent on the bulk of the inhibitor. The K_m varied from 36 μM for myxothiazol, the largest inhibitor, down to ~3 μM with mucidin, the smallest inhibitor. This latter value was the same as that observed in the absence of any Q_o-site inhibitor, either when antimycin alone was present to stimulate SO production or when turnover was measured in the absence of inhibitors, indicating that formation of the ES-complex was determined by the same kinetic parameters. This correlation between K_m and inhibitor size was extended by computational studies in which the volume overlap between the inhibitors and a UQ-1 test substrate was modeled using crystallographic structures. With a 3 Å adjustment of UQ-1 away from the position indicated by stigmatellin, which involved rotation of the Glu-272 ligand, it was possible to fit the inhibitor into the proximal domain with either no overlap (for mucidin) or partial overlap (increasingly for MOA-stilbene, famoxadone, and myxothiazol) with UQ-1, in line with the increasing K_m values. These structural considerations therefore support the hypothesis that the ES-complex can be formed in the presence of proximal domain inhibitors, since the overlaps in volume correlated well with the K_m values measured. However, the inhibitor volumes used were based on those in the structures containing inhibitors, which show substantial conformational changes compared with the native or stigmatellin-containing

structures. Possible constraints from interaction with the protein were omitted from the modeling and were therefore not reflected in the overlap values.

The SO production that is insensitive to proximal domain inhibitors must indicate some double occupancy, but the question remains of how pertinent the data are to mechanism. It is by no means obvious that the occupancy of the ES-complex with the smaller inhibitors can be used to justify a double-occupancy mechanism under normal turnover. The 12-fold change in K_m for QH_2 with myxothiazol indicates a strong impediment to occupancy of the distal domain when the proximal domain is occupied by a species with a tail; this clear evidence for a constraint on double occupancy is more pertinent to occupancy by two quinone species.

These studies demonstrated that this physiologically important reaction is experimentally accessible and that our understanding of the mechanism is intimately linked to our understanding of the mechanism of QH_2 oxidation at the Q_o-site.

MITOCHONDRIAL MYOPATHIES MAPPING TO THE BC_1 COMPLEX Mitochondrial myopathies have been extensively reviewed recently (8–11), and the relation between mitochondrial dysfunction and disease is well established. For those myopathies linked to mutation of the cyt *b* gene, many have been mapped through coding changes at the DNA level. For those leading to residue change rather than to gross truncation or deletion of sequence, the location in structural models provides a basis for detailed understanding of these diseases at the molecular level. (For a detailed discussion of the current field and of the interesting mechanistic and physiological insights provided by these mutations, see 8, 9).

Quinone Reduction at the Q_i-Site

STRUCTURAL CONSIDERATIONS Several structures are available from different labs showing the native occupant, presumably ubiquinone (2, 39, 43, 47, 89, 149); others with the inhibitor antimycin as occupant (39, 47); and a recent structure shows NQNO at the site (47). This latter paper includes the fullest structural description of the Q_i-site yet available, either vacant (but with 4 water molecules forming an H-bonded network) (1ntz), or with quinone (1ntm), antimycin (1ntk), or NQNO (nu1) bound. Unfortunately, coordinates were not available at the time of writing. In general, the protein structure that Gao et al. (47) described was relatively indifferent to occupancy, with the vacant structure showing only 0.24 Å rmsd from the quinone-occupied structure. The inhibitor binding in all structures reported (2, 39, 47, 89, 149–151) showed volumes of occupancy that impinge on the surfaces at which mutational changes (152) lead to resistance.

All structures show that the quinone is liganded directly or indirectly through H-bonds involving three side chains—His-202, Asp-229, and/or Ser-206 (chicken or yeast numbering)—and/or by structurally defined waters (39, 43, 47, 89, 153, 154). In addition, some hydrophobic or aromatic interactions with side chains and the heme edge are recognized. Interestingly, four high-resolution structures show three different configurations of side chains involved in H-bonding of the

quinone carbonyls. Most notably, His-202 is directly H-bonded to the quinone in the bovine and chicken complexes from Berry (2, 39, 147, 154) (Figure 4), but indirectly via bound water in the yeast structure described by Hunte et al. (43, 89) and the bovine complexes described by Gao et al. (47), whereas the H-bond to Asp-229 is direct in the Berry and Hunte structures, but via a water bridge in the Gao structure. An additional unpublished structure at 2.5 Å resolution from Iwata (153) is described as showing direct H-bonds with both the aspartate and histidine, as in the Berry structures. Differences are also apparent in the Ser-206 liganding, with the side chain within H-bonding distance in some structures, connected to either of the $-OCH_3$ O-atoms, and too far away in others. When considering these differences, note that the occupancy by quinone in all the structures is relatively low and that the B factors are relatively high, indicating a degree of uncertainty in assignment of the electron densities. The site is also quite spacious, allowing occupancy by a variety of inhibitors with overlapping volumes, and may allow alternative configurations for the quinone. The differences show an obvious structural plasticity, but beg the question of mechanistic relevance.

An alternative approach to mechanistically important structural features is through use of pulsed EPR or ENDOR to explore the structure around the semiquinone bound at the Q_i-site through the magnetic interaction between neighboring nuclear magnets and the paramagnetic center (154–156). Exchangeable protons contributing to H-bonds with the SQ in the bovine mitochondrial complex were identified using ENDOR and H/D exchange (157). The spectra were interpreted as showing several H-bonds, but the spectral range limited the study to the proton region. Pulsed EPR has been used to study the bc_1 complex from *Rb. sphaeroides* (158), allowing exploration of neighboring ^{14}N nuclei. ESEEM and HYSCORE spectra provided an unambiguous demonstration of a N-ligand, interpreted as an H-bond to a histidine imidazole nitrogen, likely His-217, equivalent to His-202 of mitochondria complex. This supports the Berry structures as showing a functional configuration and opens the possibility of a dynamic role of the histidine. Spectra measured using ESEEM and HYSCORE, with H_2O or ^2H_2O as the medium solvent, resolved at least two (probably three) exchangeable protons affecting the SQ spin relaxation, likely contributing to H-bonds (D.R.J. Kolling, J.T. Holland, R.I. Samoilova, S.A. Dikanov, & A.R. Crofts, unpublished). The two strongest of these likely reflect the direct H-bonds to the ring carbonyl O-atoms observed in ^{14}N-ESEEM and the crystallographic structures, although firmer attribution to particular bonds must await further work using isotopic substitutions at other atoms.

OVERVIEW OF MECHANISM OF ELECTRON TRANSFER AT THE Q_i-SITE Any mechanism must account for the fact that the Q_i-site operates as an interface between the one-electron chemistry of the *b*-heme chain, and the two-electron chemistry of the quinone pool. In addition, pathways for uptake of two protons and for exchange of substrate and product need to be identified. It is generally supposed that the site operates through a two-electron gate in which heme b_H reduces Q to SQ on one turnover of the Q_o-site, and SQ to QH_2 on a second turnover (50, 57). The

structures provide important clues to these functions. In particular, they show the groups involved in binding, and accessibility to the site from aqueous and lipid phase.

THE ROLE OF THE SEMIQUINONE AT THE Q_i-SITE Under normal turnover, the initial state of occupancy will depend on ambient redox potential and pH. A stable semiquinone is generated at the site on redox titration over the E_h range 30–60 mV higher than the E_m of the quinone pool ($E_{m,\,pool} \sim 90$ mV at pH 7), and is stabilized as the pH is raised over the range 7–9 (60, 154, 155). The SQ intermediate can also be generated by coulometric titration using a one-electron mediator (156), or by reversal of the second electron transfer (61, 145, 158). However, details of the equilibrium and rate constants, the interaction between semiquinone and heme b_H, and the specific role of ligands in this reverse reaction are unresolved (2, 125, 159–161). In each of these approaches, the yield of SQ, whether measured kinetically or thermodynamically, has always been substantially less ($\sim$0.5/heme b_H under conditions giving maximal yield) than the stoichiometry of bc_1 complex. Early work from Palmer's lab had suggested an explanation—this might reflect spin silencing from magnetic interaction with oxidized heme b_H (156). In this case, two populations of SQ might be expected, one with a fast, and the other with a slow relaxation. The thermodynamic and spectroscopic properties reported in the literature are those of a slowly relaxing species, easily saturated at temperatures $<$100 K.

The thermodynamic properties of the semiquinone have been explained in the context of the disproportionation reaction, and values for binding constants for the three species of the $Q/SQ/QH_2$ system, E_m values for the semiquinone couples for bound and unbound states, and pK values for the protolytic reactions have been proposed (60, 154, 155). In this discussion, it has been assumed that the disproportionation reactions of the bound and unbound couples reach equilibrium, but since structures became available, there has been little discussion of how this might occur at a site that appears too small to contain more than one species. The Q_i-site catalyzes a quinol-quinone transhydrogenase reaction that allows transfer from exogenous quinol to bound quinone or between exogenous quinones (162, 163). A plausible mechanism would be one in which two electrons from a donor Q_dH_2 are stored in the two *b*-hemes, allowing dissociation of the Q_d and its replacement by an acceptor Q_a, which would then leave the site as Q_aH_2 (162, 163). The rate of such a reaction would depend strongly on the probability of populating the $b_H^- b_L^-$ state. The unfavorable equilibrium constant for reduction of heme b_L through b_H (123, 126, 164) would account for the relatively slow rate observed, but this would likely be sufficient to allow equilibration of the Q and QH_2 components of the disproportionation reaction on the time scale of a redox titration. If equilibration through one-electron transfer processes occurs, it is presumably through direct or indirect interaction with mediators. The conditions used to assay semiquinone by EPR (high concentrations of redox mediators and a long equilibration time) are designed to encourage the equilibria of the disproportionation reaction, but they may

not accurately reflect the kinetically important intermediate states. Furthermore, if the semiquinone signal at the Q_i-site is modulated by magnetic interaction with the spin of oxidized cytochrome b_H (156, 161), this might lead not only to loss of amplitude, but also to some displacement of the maximum of the bell-shaped titration curve. Since the latter data are important in calculation of thermodynamic parameters, a substantial miscounting of the SQ could lead to misleading values over portions of the pH/E_h titration surface.

In discussing the mechanistic role of the semiquinone, it is necessary to take account of the equilibration of the Q/QH_2 couple with heme b_H through one-electron transfer reactions. Reduction of heme b_H through the Q_i-site by exogenous quinones, with generation of a semiquinone, occurs on addition of quinol substrate to the oxidized complex in the presence of myxothiazol. In a definitive study by de Vries et al. (61), reduction by duroquinol was rapid, with the reaction ~90% complete at the first point of measurement at 5 ms (using 300 μM QH_2). From this, a value of $\tau < 3$ ms seems appropriate. The measured rate was more rapid than the reaction through the Q_o-site monitored through the reduction of heme b_H in the presence of antimycin. The rate was also more rapid than that reported for the transhydrogenase reaction ($\tau \sim 170$ ms at 50 μM duroquinol, 163). From this, it seems likely that duroquinol, and presumably other quinols, could react directly at the Q_i-site by exchange with the initial occupant. In chromatophores, where the reactions using the native substrate can be followed *in situ*, the myxothiazol-insensitive reduction of heme b_H on generation of 1 QH_2 in the oxidized pool occurred with $\tau \sim 3$ ms (165, 166). This rate was similar to that for QH_2 oxidation through the Q_o-site under these conditions, suggesting a similar rate constant, but in both cases, the rate was limited by the delivery of QH_2 to the complex from the RC (50, 165).

For all these kinetically determined reactions, it is clear that the relevant equilibrium constants must include participation of heme b_H in the one-electron transfer reactions. One approach to determining these is through the phenomena associated with the cyt b_{150} component. This high-potential form of heme b_H has been recognized phenomenologically for over 30 years, having been observed in redox titrations of mitochondria and chromatophores in the early 1970s (164, 167). A hint as to the mechanism came from the observation that antimycin addition induced oxidation of this component (168) or eliminated it from redox titrations (125, 154, 155). In the presence of antimycin, the absorbance due to the cyt b_{150} form was lost and reappeared in the heme b_H titrating at $E_{m,7} \sim 50$ mV. The antimycin-induced oxidation of cyt *b* was explained through the following mechanism (168):

$$\text{cyt}b_H^- \cdot \text{QH}^\bullet(\text{H}^+) \leftrightarrow \text{cyt}b_H \cdot \text{QH}_2 \overset{\text{QH}_2}{\leftrightarrow} \text{cyt}b_H \cdot \text{vacant} \overset{\text{AA}}{\leftrightarrow} \text{cyt}b_H \cdot \text{AA}. \qquad 6.$$

By analogy with the well-characterized inhibitor-induced electron transfers in the Q_AQ_B sites of reaction centers and photosystem II (57), we suggested that the semiquinone at the Q_i-site accepts an electron from ferrocytochrome b_H and leaves

as the quinol, so that the oxidized form of cyt *b* is stabilized by antimycin binding. Conversely, the cyt b_{150} form must arise from a reversal of the left-hand pair of reactions, as seen experimentally from the myxothiazol-insensitive reduction of heme b_H and generation of semiquinone on addition of QH_2 to the isolated complex (61, 145, 158), or the reduction of b_H on photoreduction of the pool in chromatophores (165, 166). For the reduction of heme b_H on flash activation in chromatophores, the observed equilibrium constant precluded mechanisms involving reduction of two heme b_H centers by the Q/QH_2 couple at the E_m values found by titration, and the alternative reaction, in which QH_2 reduced heme b_H with generation of SQ, was suggested (165).

The properties of cyt b_{150} in the mitochondrial complex have been explored in detail by Rich et al. (161), and discussed in terms of differential affects of occupancy by Q, SQ, or QH_2 on the E_m of heme b_H (see 160). A set of parameters that accounted successfully for the properties of both the SQ and cyt b_{150} was proposed; however, in deriving this set, Rich et al. (161) had to assume that SQ generated in the presence of oxidized heme b_H was EPR silent owing to magnetic quenching (see 156). An alternative approach to explaining the properties of cyt b_{150} has been through the equilibria associated with reversal of the forward reaction (165), as discussed below.

THE ROLE OF CYT B_{150} IN THE MECHANISM OF THE Q_i-SITE The properties of cyt b_{150} suggest that the Q_i-site catalyzes the following reaction, in which the cyt b_{150} is represented by the state cyt b_H^- $QH^\bullet$ (125, 159, 165, 168). The reaction (Equation 7) can be considered as a reversal of the normal forward reaction by which ferroheme b_H reduces SQ to QH_2, and after release of the product, binds Q to re-establish the starting state for the Q_i-site.

$$QH_2(\text{pool}) + \text{cyt}b_HQ \leftrightarrow Q(\text{pool}) + \text{cyt}b_H^-QH^\bullet(H^+), \qquad 7.$$

Partial reactions giving rise to the overall process of Equation 7 are

$$QH_2(\text{pool}) + \text{cyt}b_HQ \leftrightarrow Q(\text{pool}) + \text{cyt}b_HQH_2, \qquad 7a.$$

$$\text{cyt}b_HQH_2 \leftrightarrow \text{cyt}b_H^-QH^\bullet(H^+), \qquad 7b.$$

At any defined pH, the equilibrium constant for formation of the cyt b_{150} form, obtained from the partial processes of Equations 7*a* and 7*b*, is given by

$$K_{eq} = K_{7a}K_{7b} = (K_{A(QH_2)}/K_{A(Q)})\exp\{(E_{m(\text{cyt}b_H)} - E_{m(QH^\bullet/QH_2)}F/RT)\}, \qquad 8.$$

where K_A values are association (binding) constants for QH_2 and Q, and $E_{m(\text{cyt}bH)}$ and $E_{m(QH^\bullet/QH_2)}$ refer to the mid-point potentials of cyt b_H, and of the SQ/quinol couple bound at the site, respectively.

Examination of Equation 8 shows that an increased value of K_{eq} could be expected if $E_{m(\text{cyt}bH)}$ is increased, if $E_{m(QH^\bullet/QH_2)}$ is decreased, if the affinity of quinol is increased, or if the affinity of quinone is decreased. However, the affinities for Q and QH_2 have an importance that can be expressed in a different form. When

expressed with respect to the potential of the quinone pool, the ratio of binding constants for Q and QH_2 contributes to the value for $E_{m(QH^{\bullet}/QH_2)}$ in such a way as to cancel the pre-exponential term. This gives

$$K_{eq} = \exp\{E_{m(cytb_H)} + E_{m(Q/QH^{\bullet})} - 2E_{m(Q_{pool})}\}F/RT, \qquad 9.$$

where $E_{m(Q/QH^{\bullet})}$ refers to the bound couple. This same expression can also be derived directly from Equation 6 using the conventional relationship between equilibrium constant and half-cell potentials. Incorporation of this equation in a computer model allows exploration of the variation of redox states of all components as a function of redox potential, pH, etc. (125). Interestingly, the properties of the cyt b_{150} phenomena are reproduced quite well using measured values for E_m and pK for heme b_H, reasonable values for binding constants (with a ratio of ~100 in favor of QH_2), and E_m values for the $Q/SQ/QH_2$ system derived from redox titrations and kinetic experiments (125). The properties of the SQ are also reproduced quite well, but are mechanistically linked to formation of SQ through reaction 6 above, so that the SQ observed is in the form cyt $b_H^- \cdot QH^{\bullet}$. An interesting feature of these simulations was that, because of the importance of E_m of heme b_H in Equation 9, the pH dependence of both b_{150} and the SQ were well explained, but are determined by the pK at ~7.8 on the heme b_H, without invoking a pK in the neutral range for the semiquinone (M. Guergova-Kuras & A.R. Crofts, unpublished).

Support for the above mechanisms also comes from analysis of strains with mutations in the Q_i-site. We have previously noted that in two mutants in which the E_m of cytochrome b_H was lowered, but by residue changes removed from the catalytic domain, the amount of cytochrome b_{150} was substantially decreased (124, 125, 169). This trend was apparent in mutants N223V, G220V, S218A, and N222A (all with lowered E_m for cyt b_H), which showed a reduced level of cyt_{150} (169). Similarly, in T219A and in a double mutant K251D/D252K (which had higher E_m values) the level of cyt_{150} was enhanced (125).

Although this simple model explains much of the data, in other mutants, including some showing higher levels of cytochrome b_{150} but a lower E_m for cyt b_H than wild type, the change in relative stability could not be attributed simply to changes in E_m of cytochrome b_H and would have to be explained in terms of changes in the other parameters of equation (125, 169). A lack of correlation between the amount of cytochrome b_{150} and the stability of the EPR-detectable semiquinone at the Q_i-site has also been noted in a series of mutants in the bc_1 complex of *Rb. capsulatus* (166). These departures from the simple model presented here are not unexpected, but suggest that the role of semiquinone stability needs to be explored more fully. Note that the role of protons in equilibrium with the partial reactions has not been explored. Changes in kinetics and in the equilibrium constants combined in K_{eq} in Equation (8) could reflect these protolytic equilibria, and the kinetics of the proton processing accompanying redox turnover. The relationship between cytochrome b_{150}, the semiquinone, and the protolytic equilibria clearly require further investigation.

THE FORWARD REACTION As noted above, the operation of the two-electron gate at the Q_i-site is associated with a relatively stable SQ intermediate, and the mechanism is described by a set of equilibrium and rate constants defining the electron transfer reactions and the binding of Q and QH_2 from the pool. These also determine the properties of cyt b_{150}. In pre-steady-state kinetic experiments with the *Rb. sphaeroides* complex in situ, electron transfer rates in the forward direction through the *b*-heme chain to the Q_i-site are faster than the rate-limiting step. Since complete turnover delivers two electrons in succession to the Q_i-site (50, 54), this holds for electron transfer to both endogenous Q and SQ species. The fact that the observed rate is that of the limiting step at the Q_o-site restricts use of the kinetic data to estimation of upper limits for the forward rate constants. With the quinone pool initially oxidized (and the site presumably occupied by Q), cyt b_H remains partly reduced in the 100-ms range after generation of one QH_2 in the pool by flash excitation of the RC, suggesting an equilibrium constant for reduction of Q by heme b_H^- with $K_{eq} \sim 3$, in the range expected from the E_m of heme b_H, and the value for E_m Q/QH$^\bullet$ from simulation. This relatively stable level of heme b_H reduction is seen when the pool is initially oxidized, but titrates away as the pool starts to become reduced over the range below $E_{h,7}$ 150 mV, so that at 100 mV, reoxidation of heme b_H is complete. Over this same range, cyt b_{150} (likely the state cyt $b_H^- \cdot$ QH$^\bullet$, as discussed above) is formed in the pre-flash equilibrium mix, as determined by the equilibria shown in Equation 10. This brings up the question of the state of the Q_i-site under these conditions.

$$\begin{array}{c} \text{Q to pool} \\ \curvearrowright \\ \text{cyt}b_L\text{cyt}b_H\text{Q} \leftrightarrow \text{cyt}b_L\text{cyt}b_H[\text{vac}] \underset{\curvearrowleft}{\leftrightarrow} \text{cyt}b_L\text{cyt}b_H\text{QH}_2 \leftrightarrow \text{cyt}b_L\text{cyt}b_H^-\text{QH}^\bullet. \\ \text{QH}_2 \text{ from pool.} \end{array} \quad 10.$$

At potentials around the midpoint of the Q-pool a substantial fraction of Q_i-sites (depending on pH) will be in the cyt b_{150} state, suggesting a forward reaction according to Equations 11 and 12:

$$\begin{array}{c} e^- \text{ from first } QH_2 \text{ at } Q_o\text{-site} \\ \curvearrowright \\ \text{cyt}b_L\text{cyt}b_H^-\text{QH}^\bullet \leftrightarrow \text{cyt}b_L^-\text{cyt}b_H^-\text{QH}^\bullet \leftrightarrow \text{cyt}b_L\text{cyt}b_H^-\text{QH}_2 \underset{\curvearrowleft}{\leftrightarrow} \text{cyt}b_L\text{cyt}b_H^-[\text{vac}]. \\ \text{QH}_2 \text{ to pool.} \end{array} \quad 11.$$

$$\begin{array}{c} e^- \text{ from second } QH_2 \text{ at } Q_o\text{-site} \\ \curvearrowright \\ \text{cyt}b_L\text{cyt}b_H^-[\text{vac}] \underset{\curvearrowleft}{\leftrightarrow} \text{cyt}b_L\text{cyt}b_H^-\text{Q} \leftrightarrow \text{cyt}b_L\text{cyt}b_H\text{QH}^\bullet \leftrightarrow \text{cyt}b_L\text{cyt}b_H^-\text{QH}^\bullet. \\ \text{Q from pool.} \end{array} \quad 12.$$

If the rate constants for formation of the cyt b_{150} state (Equation 10) are rapid compared with the rate-limiting step, as seems quite possible from the data, then it is likely that most centers follow the pathway shown by Equations 11 and 12 under conditions in which QH_2 is initially available in the pool. In contrast to conventional schemes, the acceptor of the first electron at the Q_i-site would be the SQ, and the second electron would reduce Q to SQ to regenerate the starting state [see Slater (145) for an earlier discussion]. Since the bc_1 complex shows a maximal rate with the pool half reduced, and since under the coupled steady-state the pool is also partly reduced, this would represent the more physiologically important pathway for turnover.

The sequence of reactions 9 to 11, starting with the oxidized complex, also provides a basis for understanding the multiphasic reduction of heme b_H seen on addition of exogenous quinol reductants to the oxidized complex (61, 81, 95, 170). The initial rapid phase, which is antimycin sensitive and myxothiazol insensitive (61), would correspond to reaction 9. Then, from the perspective of heme b_H, the reaction of Equation 11 would represent a lag, and the reactions of Equation 11 would give an oxidative phase followed by a reductive phase with kinetics similar to the slower phase of reduction of cyt c_1, as observed (61).

LIGANDS OF MECHANISTIC IMPORTANCE Consideration of two higher resolution crystallographic structures available at the time, and their EPR data, led Kolling et al. (158) to interpret the structural differences in the Q_i-site as reflecting changes in ligation for the different quinone species during the catalytic cycle, and a dynamic role for His-202 in transfer of protons and water into the site. This led to a scheme for the sequence of reactions involved in the forward electron transfer as shown in Figure 5. An alternative model has been suggested by Gao et al. (47), in which all bound quinone species are H-bonded through bridging waters (as shown by the quinone in their structure) during the catalytic cycle. This model is incompatible with the EPR data showing a direct H-bond between SQ and a histidine N. However, the structures proposed by Gao et al. (47) fit quite naturally into the scheme of Figure 5, providing a water-filled vacant site (*F*), and an intermediate between the vacant state (*G*) and quinone-bound states seen in the structures of Hunte (43, 89) (*A*) and Berry (2, 39, 147, 154) (*B*), prior to formation of the semiquinone in the environment seen by ESEEM (154) (*C*).

ACCESS TO THE QUINONE BINDING SITE OF SUBSTRATE, WATER, AND PROTONS Structures for the vacant site show waters in the volume of the quinone, and all high-resolution structures have water in addition to the quinone within the site. For example, in addition to waters involved in H-bonds to the quinone, Ser-206 in the structures of both Hunte (43, 89) and Berry (154) forms an H-bond to a water that also forms an H-bond to a heme propionate, and both structures show waters that seem to be "caught in the act" of communication between the internal volume and the external phase through a small hole bordered by His-202.

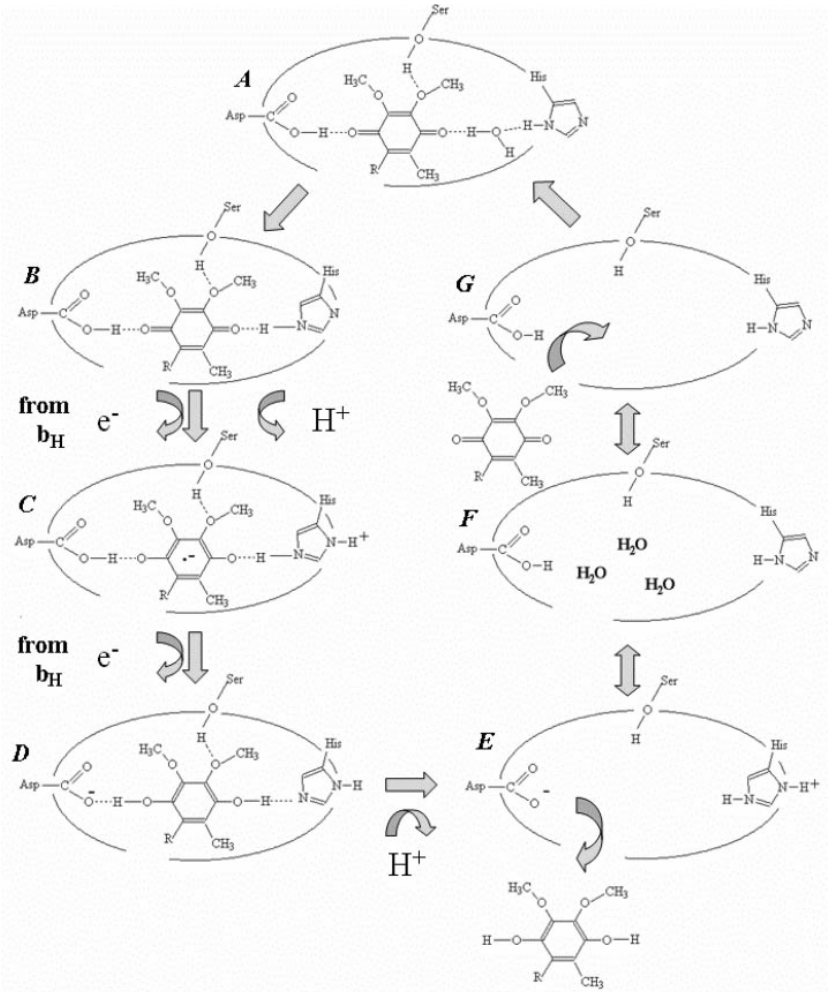

Figure 5 Scheme showing proposed involvement of liganding groups in the function of the Q_i-site (adapted from 158). The different occupants of the site are shown for different states of the cycle of reactions at the Q_i-site, shown in the direction of forward electron flow. State ***A*** might represent Hunte's structure (43), state ***B*** Berry's structure (see Figure 4), and state ***C*** the structure determined by Kolling et al. (158) using ESEEM. The vacant site with waters would correspond to the vacant site in Gao et al. (47), and their quinone-occupied site would be intermediate between ***G*** and ***A***. The arrows show the direction of forward electron transfer. Reversal of the second electron transfer leading to formation of the semiquinone from QH_2 in addition to the oxidized complex would be represented by reversal of transitions leading to formation of state ***A*** from ***C***. No attempt has been made to show the many different states of protonation of the residues involved, and the particular points of entry of H^+ in the scheme should therefore be regarded as flexible and would change with pH.

Lange et al. (89) discussed at length a possible role for waters around the site in transfer of H^+ into the site, and their relation to exterior waters and phospholipid. For the lipid phase, the quinone and inhibitor tails provide an Ariadne's thread, showing the path into the site from the lipid through a fairly wide access channel.

INTERACTIONS BETWEEN THE MONOMERS A clear role for the dimeric structure lies in binding of the ISP N-terminal anchor so as to allow the cross-dimer interactions of the mobile head (65). The mechanistic discussions above have focused on models in which all reactions are within a monomer, but there have been many speculations about mechanisms involving dimeric Q-cycles and control through interactions between monomers in the dimeric complex (3, 38, 40, 60–62, 83, 86, 88, 145, 162, 171). Most of the tantalizing evidence for mechanistic interactions has come from work on mitochondrial complexes. Work from the author's lab in collaboration with Dr. Vlad Shinkarev to explore such interactions in the bacterial system has so far failed to provide any compelling evidence for electron transfer between monomers, or control by allosteric interactions across the dimer interface (unpublished). Possibly, the additional subunits of the mitochondrial complexes have evolved to provide a means for fine-tuning the mechanism through such interactions.

THE PHYSIOLOGICAL PERSPECTIVE Although most attention has been paid to the Q_o-site, the Q_i-site has also been discussed as a possible site for SO generation, and a number of myopathies in cyt *b* have mapped to the site (8, 9). The well-established effect on SO production of blocking the Q_i-site, as in the antimycin stimulation, has led to some confusion, because antimycin is specific for the Q_i-site, and might have led to the conclusion that this site has an important role in SO production. More plausible is a mechanism based on a Q_o-site generation, stimulated by back-up in the *b*-heme chain. The relatively high redox potential of the semiquinone couples consequent on the stability of the Q_i-site SQ would make them unlikely donors in the production of superoxide.

Although the Q_o-site inhibitors have attracted most attention in clinical and agronomical applications, the species-selectivity of the Q_i-site is another attractive target that remains to be exploited.

ACKNOWLEDGMENTS

Support for the author's research from the following sources is gratefully acknowledged: NIH (GM 35438 to A.R.C., GM 62954 to Sergei Dikanov.), and a Fogarty grant (PHS 1 R03 TW01495, with Rimma Samoilova). The views presented are those of the author unless otherwise indicated. Helpful discussions with the following are gratefully acknowledged: Vlad Shinkarev, Ed Berry, Sergei Dikanov, Rimma Samoilova, Judy Hirst, Uli Brandt, Peter Rich, Hildur Palsdottir, Bernie Trumpower, Raúl Covián, Carola Hunte, David Kramer, and Florian Muller.

The *Annual Review of Physiology* is online at http://physiol.annualreviews.org

LITERATURE CITED

1. Crofts AR, Berry EA. 1998. Structure and function of the cytochrome bc_1 complex of mitochondria and photosynthetic bacteria. *Curr. Opin. Struct. Biol.* 8: 501–9
2. Berry E, Guergova-Kuras M, Huang L-S, Crofts AR. 2000. Structure and function of cytochrome *bc* complexes. *Annu. Rev. Biochem.* 69:1007–77
3. Hunte C, Palsdottir H, Trumpower BL. 2003. Protonmotive pathways and mechanisms in the cytochrome bc_1 complex. *FEBS Lett.* 545:39–46
4. Cramer WA, Soriano GM, Ponomarev M, Huang D, Zhang H, et al. 1996. Some new structural aspects and old controversies concerning the cytochrome b6f complex of oxygenic photosynthesis. *Annu. Rev. Plant Physiol. Plant Mol. Biol.* 47:477–508
5. Woese CR. 1987. Bacterial evolution. *Microbiol. Rev.* 51:221–71
6. Nitschke W, Muehlenhoff U, Liebl U. 1997. Evolution. In *Photosynthesis: A Comprehensive Treatise*, ed. A Raghavendra, pp. 285–304. Cambridge, UK: Cambridge Univ. Press
7. Degli Esposti M, de Vries S, Crimi M, Ghelli A, Patarnello T, Meyer A. 1993. Mitochondrial cytochrome b: evolution and structure of the protein. *Biochim. Biophys. Acta* 1143:243–71
8. Fisher N, Meunier B. 2001. Effects of mutations in mitochondrial cytochrome *b* in yeast and man—deficiency, compensation and disease. *Eur. J. Biochem.* 268:1155–62
9. Fisher N, Meunier B. 2002. The bc_1 complex: structure, function and dysfunction. In *Recent Research Developments in Human Mitochondrial Myopathies*, ed. J Garcia-Trejo, pp. 97–112. Kerala, India: Research Signpost
10. Rose MR. 1998. Mitochondrial myopathies. Genetic mechanisms. *Arch. Neurol.* 55:17–24
11. Vogel H. 2001. Mitochondrial myopathies and the role of the pathologist in the molecular era. *J. Neuropathol. Exp. Neurol.* 60:217–27
12. Boveris A. 1984. Determination of the production of superoxide radicals and hydrogen-peroxide in mitochondria. *Methods Enzymol.* 105:429–35
13. Turrens JF, Alexandre A, Lehninger AL. 1985. Ubisemiquinone is the electron donor for superoxide formation by complex III of heart mitochondria. *Arch. Biochem. Biophys.* 237:408–14
14. Skulachev VP. 1996. Role of uncoupled and non-coupled oxidations in maintenance of safely low levels of oxygen and its one-electron reductants. *Q. Rev. Biophys.* 29:169–202
15. Muller F. 2000. The nature and mechanism of superoxide production by the electron transport chain: its relevance to aging. *J. Am. Aging Assoc.* 23:227–53
16. Chen Q, Vazquez EJ, Moghaddas S, Hoppel CL, Lesnefsky EJ. 2003. Production of reactive oxygen species by mitochondria: central role of Complex III. *J. Biol. Chem.* 278: 36027–31
17. Kristal BS, Jackson CT, Chung HY, Matsuda M, Nguyen HD, Yu BP. 1997. Defects at center P underlie diabetes-associated mitochondrial dysfunction. *Free Radic. Biol. Med.* 22:823–33
18. Hoek TLV, Shao ZH, Li CQ, Schumacker PT, Becker LB. 1997. Mitochondrial electron transport can become a significant source of oxidative injury in cardiomyocytes. *J. Mol. Cell. Cardiol.* 29:2441–50
19. Harman D. 1992. Free radical theory of aging: history. *EXS* 62:1–10
20. Ames BN, Shigenaga MK, Hagen TM. 1993. Oxidants, antioxidants, and the

degenerative diseases of aging. *Proc. Natl. Acad. Sci. USA* 90:7915–21
21. Beckman KB, Ames BN. 1998. The free radical theory of aging matures. *Physiol. Rev.* 78:547–81
22. Raha S, Robinson BH. 2001. Mitochondria, oxygen free radicals, and apoptosis. *Am.J. Med. Genet.* 106:62–70
23. Orth M, Schapira AHV. 2001. Mitochondria and degenerative disorders. *Am. J. Med. Genet.* 106:27–36
24. Papa S, Skulachev VP. 1997. Reactive oxygen species, mitochondria, apoptosis and aging. *Mol. Cell. Biochem.* 174:305–19
25. Bowyer JR, Dutton PL, Prince RC, Crofts AR. 1980. The role of the Rieske iron-sulfur center as the electron donor to ferricytochrome c_2 in *Rhodopseudomonas sphaeroides*. *Biochim. Biophys. Acta* 592:445–60
26. Meinhardt SW, Crofts AR. 1982. The site and mechanism of action of myxothiazol as an inhibitor of electron transfer in *Rhodopseudomonas sphaeroides*. *FEBS Lett.* 149:217–22
27. von Jagow G, Link T. 1988. Use of specific inhibitors on the mitochondrial bc_1 complex. *Methods Enzymol.* 126:253–71
28. Brandt U, Schagger H, von Jagow G. 1988. Characterization of binding of the methoxyacrylate inhibitors to mitochondrial cytochrome c reductase. *Eur. J. Biochem.* 173:499–506
29. Tsai A-L, Kauten R, Palmer G. 1985. The interaction of yeast Complex III with some respiratory inhibitors. *Biochim. Biophys. Acta* 806:418–26
30. Link TA, Haase U, Brandt U, von Jagow G. 1993. What information do inhibitors provide about the structure of the hydroquinone oxidation site of ubiquinol:cytochrome *c* oxidoreductase. *J. Bioenerg. Biomembr.* 25:221–32
31. Slater EC. 1973. The mechanism of action of the respiratory inhibitor, antimycin. *Biochim. Biophys. Acta* 301:129–54
32. Srivastava IK, Morrisey JM, Darrouzet E, Daldal F, Vaidya AB. 1999. Resistance mutations reveal the atovaquone-binding domain of cytochrome *b* in malaria parasites. *Mol. Microbiol.* 33:704–11
33. Beautement K, Clough JM, Defraine PJ, Godfrey CRA. 1991. Fungicidal Betamethoxyacrylates—from natural products to novel synthetic agricultural fungicides. *Pestic. Sci.* 31:499–519
34. Clough JM, Godfrey CRA. 1995. Growing hopes. *Chem. Br.* 31:466–69
35. Bartlett DW, Clough JM, Godwin JR, Hall AA, Hamer M, Parr DB. 2002. The strobilurin fungicides. *Pest-Manage. Sci.* 58:649–62
36. Sauter H, Ammermann E, Roehl F. 1996. Strobilurins—from natural products to a new class of fungicides. In *Crop Protection Agents from Nature*, ed. LG Copping, pp. 50–81. Cambridge, UK: Thomas Graham House, R. Soc. Chem.
37. Yu C-A, Xia J-Z, Kachurin AM, Yu L, Xia D, et al. 1996. Crystallization and preliminary structure of beef heart mitochondrial cytochrome-bc_1 complex. *Biochim. Biophys. Acta* 1275:47–53
38. Xia D, Yu C-A, Kim H, Xia J-Z, Kachurin AM, et al. 1997. Crystal structure of the cytochrome bc_1 complex from bovine heart mitochondria. *Science* 277:60–66
39. Zhang Z, Huang L-S, Shulmeister VM, Chi Y-I, Kim K-K, et al. 1998. Electron transfer by domain movement in cytochrome bc_1. *Nature* 392:677–84
40. Iwata S, Lee JW, Okada K, Lee JK, Iwata M, et al. 1998. Complete structure of the 11-subunit bovine mitochondrial cytochrome bc_1 complex. *Science* 281:64–71
41. Kim H, Xia D, Yu C-A, Xia JZ, Kachurin AM, et al. 1998. Inhibitor binding changes domain mobility in the iron-sulfur protein of the mitochondrial bc_1 complex from bovine heart. *Proc. Natl. Acad. Sci. USA* 95:8026–33
42. Yu C-A, Xia D, Kim H, Deisenhofer J, Zhang L, et al. 1998. Structural basis of functions of the mitochondrial

cytochrome bc_1 complex. *Biochim. Biophys. Acta* 1365:151–58
43. Hunte C, Koepke J, Lange C, Rossmanith T, Michel H. 2000. Structure at 2.3 Å resolution of the cytochrome bc_1 complex from the yeast *Saccharomyces cerevisiae* co-crystallized with an antibody Fv fragment. *Structure* 8:669–84
44. Gao X, Wen X, Yu C-A, Esser L, Tsao S, et al. 2002. The crystal structure of mitochondrial cytochrome bc_1 in complex with famoxadone: the role of aromatic-aromatic interaction in inhibition. *Biochemistry* 41:11692–702
45. Palsdottir H, Lojero CG, Trumpower BL, Hunte C. 2003. Structure of the yeast cytochrome bc_1 complex with a hydroxyquinone anion Q_o site inhibitor bound. *J. Biol. Chem.* 278: 31303–11
46. Kessl JJ, Lange BB, Merbitz-Zahradnik T, Zwicker K, Hill P, et al. 2003. Molecular basis for atovaquone binding to the cytochrome bc_1 complex. *J. Biol. Chem.* 278: 31312–18
47. Gao X, Wen X, Esser L, Quinn B, Yu L, Yu C-A, Xia D. 2003. Structural basis for the quinone reduction in the bc_1 complex: a comparative analysis of crystal structures of mitochondrial cytochrome bc_1 with bound substrate and inhibitors at the Q_i site. *Biochemistry.* 42:9067–80
48. Zhang HM, Kurisu G, Smith JL, Cramer WA. 2003. A defined protein-detergent-lipid complex for crystallization of integral membrane proteins: the cytochrome b_6f complex of oxygenic photosynthesis. *Proc. Natl. Acad. Sci. USA* 100:5160–63
49. Mitchell P. 1976. Possible molecular mechanisms of the protonmotive function of cytochrome systems. *J. Theor. Biol.* 62:327–67
50. Crofts AR, Meinhardt SW, Jones KR, Snozzi M. 1983. The role of the quinone pool in the cyclic electron-transfer chain of *Rhodopseudomonas sphaeroides*: a modified Q-cycle mechanism. *Biochim. Biophys. Acta* 723:202–18
51. Crofts AR. 1985. The mechanism of ubiquinol: cytochrome c oxidoreductases of mitochondria and of *Rhodopseudomonas sphaeroides*. In *The Enzymes of Biological Membranes*, ed. AN Martonosi, 4:347–82. New York: Plenum
52. Crofts AR, Wang Z. 1989. How rapid are the internal reactions of the ubiquinol: cytochrome c_2 oxidoreductase? *Photosynth. Res.* 22:69–87
53. Crofts AR. 2003. The Q-cycle—a personal perspective. In The Millenium Issues on the History of Photosynthesis. *Photosynth. Res.* ed. Govindjee. In press
54. Crofts AR, Shinkarev VP, Kolling DRJ, Hong S. 2003. The modified Q-cycle explains the apparent mismatch between the kinetics of reduction of cytochromes c_1 and b_H in the bc_1 complex. *J. Biol. Chem.* 278:36191–201
55. Rich PR. 1981. Electron transfer reactions between quinols and quinones in aqueous and aprotic media. *Biochim. Biophys. Acta* 637:28–33
56. Junemann S, Heathcote P, Rich PR. 1998. On the mechanism of quinol oxidation in the bc_1 complex. *J. Biol. Chem.* 273:21603–7
57. Crofts AR, Wraight CA. 1983. The electrochemical domain of photosynthesis. *Biochim. Biophys. Acta* 726:149–86
58. Garland PB, Clegg RA, Boxer D, Downie JA, Haddock BA. 1975. Proton-translocating nitrate reductase of *Escherichia coli*. In *Electron Transfer Chains and Oxidative Phosphorylation*, ed. E Quagliariello, S Papa, F Palmieri, EC Slater, N Siliprandi, pp. 351–58. Amsterdam: North-Holland
59. King TE, Yu C-A, Yu L, Chiang Y. 1975. An examination of the components, sequence, mechanisms and their uncertainties involved in mitochondrial electron transport from succinate to cytochrome *c*. See Ref. 58, pp. 105–18
60. de Vries S, Berden JA, Slater EC. 1982. Oxidation-reduction properties of an antimycin-sensitive semiquinone anion bound to QH_2:cytochrome *c*

oxidoreductase. In *Function of Quinones in Energy Conserving Systems*, ed. BL Trumpower, pp. 235–46. New York: Academic
61. de Vries S, Albracht SPJ, Berden JA, Marres CAM, Slater EC. 1983. The effect of pH, ubiquinone depletion and myxothiazol on the reduction kinetics of the prosthetic groups of QH_2: cytochrome c oxidoreductase. *Biochim. Biophys. Acta* 723:91–103
62. de Vries S. 1983. *The pathway of electrons in QH_2 cytochrome c oxidoreductase.* PhD thesis. Amsterdam Univ., The Netherlands
63. Tsai A-L, Olson JS, Palmer G. 1983. The oxidation of yeast complex III. *J. Biol. Chem.* 258:2122–25
64. Mitchell P. 1975. Proton motive redox mechanism of the cytochrome *b*-c_1 complex in the respiratory chain: proton motive ubiquinone cycle. *FEBS Lett.* 56:1–6
65. Crofts AR, Guergova-Kuras M, Huang L-S, Kuras R, Zhang Z, Berry EA. 1999. The mechanism of ubiquinol oxidation by the bc_1 complex: the role of the iron sulfur protein, and its mobility. *Biochemistry* 38:15791–806
66. Crofts AR, Hong S, Zhang Z, Berry EA. 1999. Physicochemical aspects of the movement of the Rieske iron sulfur protein during quinol oxidation by the bc_1 complex. *Biochemistry* 38:15827–39
67. Crofts AR, Barquera B, Gennis RB, Kuras R, Guergova-Kuras M, Berry EA. 1999. The mechanism of ubiquinol oxidation by the bc_1 complex: the different domains of the quinol binding pocket, and their role in mechanism, and the binding of inhibitors. *Biochemistry* 38:15807–26
68. Tian H, White S, Yu L, Yu C-A. 1999. Evidence for the head domain movement of the Rieske iron-sulfur protein in electron transfer reaction of the cytochrome bc_1 complex. *J. Biol. Chem.* 274:7146–52
69. Tian H, Yu L, Mather MW, Yu C-A. 1998. Flexibility of the neck region of the Rieske iron-sulfur protein is functionally important in the cytochrome bc_1 complex. *J. Biol. Chem.* 273:27953–59
70. Darrouzet E. Valkova-Valchanova M, Moser CC, Dutton PL, Daldal F. 2000. Uncovering the [2Fe2S] domain movement in cytochrome bc_1 and its implications for energy conversion *Proc. Natl. Acad. Sci. USA* 97:4567–72
71. Darrouzet E, Moser CC, Dutton PL, Daldal F. 2001. Large scale domain movement in cytochrome bc_1: a new device for electron transfer in proteins. *TIBS* 26:445–51
72. Darrouzet E, Daldal F. 2003. Protein-protein interactions between cytochrome *b* and the Fe-S protein subunits during QH_2 oxidation and large-scale domain movement in the bc_1 complex. *Biochemistry* 42:1499–507
73. Crofts AR, Hong SJ, Ugulava N, Barquera B, Gennis RB, et al. 1999. Pathways for proton release during ubihydroquinone oxidation by the bc_1 complex. *Proc. Natl. Acad. Sci. USA* 96:10021–26
74. Bowyer JR, Edwards CA, Ohnishi T, Trumpower BL. 1982. An analogue of ubiquinone which inhibits respiration by binding to the iron-sulfur protein of the cytochrome bc_1 segment of the mitochondrial respiratory chain. *J. Biol. Chem.* 257:8321–30
75. Matsuura K, Bowyer JR, Ohnishi T, Dutton PL. 1983. Inhibition of electron transfer by 3-alkyl-2-hydroxy-1,4-naphthoquinones in the ubiquinol-cytochrome c oxidoreductases of *Rhodopseudomonas sphaeroides* and mammalian mitochondria. Interaction with a ubiquinone-binding site and the Rieske iron-sulfur cluster. *J. Biol. Chem.* 258:1571–77
76. Fivelman QL, Butcher GA, Adagu IS, Warhurst DC, Pasvol G. 2002. Malarone treatment failure and in vitro confirmation of resistance of *Plasmodium falciparum* isolate from Lagos, Nigeria. *Malar. J.* 1:1–4
77. Van Ark G, Berden JA. 1977. Binding of HQNO to beef-heart sub-mitochondrial

particles. *Biochim. Biophys. Acta* 459: 119–27
78. Crofts AR, Guergova-Kuras M, Kuras R, Ugulava N, Li J, Hong S. 2000. Proton-coupled electron transfer at the Q_o-site: What type of mechanism can account for the high activation barrier? *Biochim. Biophys. Acta* 1459:456–66
79. Jordan DB, Livingston RS, Bisaha JJ, Duncan KE, Pember SO, et al. 1999. Mode of action of famoxadone. *Pestic. Sci.* 55:105–18
80. Meinhardt SW, Crofts AR. 1983. The role of cytochrome b_{566} in the electron transfer chain of *Rps. sphaeroides*. *Biochim. Biophys. Acta* 723:219–30
81. Hansen KC, Schultz BE, Wang G, Chan SI. 2000. Reaction of *Escherichia coli* cytochrome bo_3 and mitochondrial cytochrome bc_1 with a photoreleasable decylubiquinol. *Biochim. Biophys. Acta* 1456:121–37
82. Schultz BE, Chan SI. 2001. Structures and proton-pumping strategies of mitochondrial respiratory enzymes. *Annu. Rev. Biophys. Biomol. Struct.* 30:23–65
83. Yu C-A, Wen X, Xiao K, Xia D, Yu L. 2002. Inter- and intra-molecular electron transfer in the cytochrome bc_1 complex. *Biochim. Biophys. Acta* 1555:65–70
84. Link TA. 1997. The role of the "Rieske" iron sulfur protein in the hydroquinone oxidation (Q_p-) site of the cytochrome bc_1 complex: the "proton-gated affinity change" mechanism. *FEBS Lett.* 412: 257–64
85. Brandt U. 1998. The chemistry and mechanics of ubihydroquinone oxidation at center P (Q_o) of the cytochrome bc_1 complex. *Biochim. Biophys. Acta* 1365:261–68
86. Snyder CH, Gutierrez-Cirlos EB, Trumpower BL. 2000. Evidence for a concerted mechanism of ubiquinol oxidation by the cytochrome bc_1 complex. *J. Biol. Chem.* 275:13535–41
87. Trumpower BL. 2002. A concerted, alternating sites mechanism of ubiquinol oxidation by the dimeric cytochrome bc_1 complex. *Biochim. Biophys. Acta* 1555:166–73
88. Lange C, Hunte C. 2002. Crystal structure of the yeast cytochrome bc_1 complex with its bound substrate cytochrome *c*. *Proc. Natl. Acad. Sci. USA* 99:2800–5
89. Lange C, Nett JH, Trumpower BL, Hunte C. 2001. Specific roles of protein-phospholipid interactions in the yeast bc_1 complex structure. *EMBO J.* 23:6591–600
90. Nett JH, Hunte C, Trumpower BL. 2000. Changes to the length of the flexible linker region of the Rieske protein impair the interaction of ubiquinol with the cytochrome bc_1 complex. *Eur. J. Biochem.* 267:5777–82
91. Xiao K, Engstrom G, Rajagukguk S, Yu C-A, Yu L, et al. 2003. Effect of famoxadone on photoinduced electron transfer between the iron-sulfur center and cytochrome c_1 in the cytochrome bc_1 complex. *J. Biol. Chem.* 278:11419–26
92. Engstrom G, Xiao K, Yu C-A, Yu L, Durham B, Millett F. 2002. Photoinduced electron transfer between the Rieske iron-sulfur protein and cytochrome c_1 in the *Rhodobacter sphaeroides* cytochrome bc_1 complex: effects of pH, temperature, and driving force. *J. Biol. Chem.* 277:31072–78
93. Hong SJ, Ugulava N, Guergova-Kuras M, Crofts AR. 1999. The energy landscape for ubihydroquinone oxidation at the Q_o-site of the bc_1 complex in *Rhodobacter sphaeroides*. *J. Biol. Chem.* 274:33931–44
94. Guergova-Kuras M, Kuras R, Ugulava N, Hadad I, Crofts AR. 2000. Specific mutagenesis of the Rieske iron sulfur protein in *Rhodobacter sphaeroides* shows that both thermodynamic gradient and the pK of the oxidized form determine the rate of quinol oxidation by the bc_1 complex. *Biochemistry* 39:7436–44
95. Snyder C, Trumpower BL. 1998. Mechanism of ubiquinol oxidation by the cytochrome bc_1 complex—pre-steady-state

kinetics of cytochrome bc_1 complexes containing site-directed mutants of the Rieske iron-sulfur protein. *Biochim. Biophys. Acta* 1365:125–34

96. Ugulava NB, Crofts AR. 1998. CD-monitored redox titration of the Rieske Fe-S protein of *Rhodobacter sphaeroides*: pH dependence of the mid-point potential in isolated bc_1 complex and in membranes. *FEBS Lett.* 440:409–13
97. Crofts AR, Berry EA, Kuras R, Guergova-Kuras M, Hong S, Ugulava N. 1998. Structures of the bc_1 complex reveal dynamic aspects of mechanism. In *Photosynthesis: Mechanisms and Effects*, ed. G Garab, 3:1481–86. Dordrecht/Boston/London: Kluwer
98. Izrailev S, Crofts AR, Berry EA, Schulten K. 1999. Steered molecular dynamics simulation of the Rieske subunit motion in the cytochrome bc_1 complex. *Biophys. J.* 77:1753–68
99. Crofts AR, Guergova-Kuras M, Ugulava N, Kuras R, Hong S. 2002. Proton processing at the Q_o-site of the bc_1 complex of *Rhodobacter sphaeroides*. *Proc. Congr. Photosynth. Res., 12th, Brisbane, Australia*, S12-002. 6 pp.
100. Ding H, Moser CC, Robertson DE, Tokito MK, Daldal F, Dutton PL. 1995. Ubiquinone pair in the Q_o site central to the primary energy conversion reactions of cytochrome bc_1 complex. *Biochemistry* 34:15979–96
101. Link TA, von Jagow G. 1995. Zinc ions inhibit the Q_P center of bovine heart mitochondrial bc_1 complex by blocking a protonatable group. *J. Biol. Chem.* 270:25001–6
102. Brandt U, Okun JG. 1997. Role of deprotonation events in ubihydroquinone: cytochrome *c* oxidoreductase from bovine heart and yeast mitochondria. *Biochemistry* 36:11234–40
103. Covián R, Moreno-Sánchez R. 2001. Role of protonatable groups of bovine heart bc_1 complex in ubiquinol binding and oxidation. *Eur. J. Biochem.* 268:5783–90
104. Link TA. 1999. The structures of Rieske and Rieske-type proteins. *Adv. Inorg. Chem.* 47:83–157
105. Colbert C, Couture MM-J, Eltis LD, Bolin JT. 2000. A cluster exposed: structure of the Rieske ferredoxin from biphenyl dioxygenase and the redox properties of Rieske Fe-S proteins. *Structure* 8:1267–78
106. Ullmann GM, Noodleman L, Case DA. 2002. Density functional calculation of pK_a values and redox potentials in the bovine Rieske iron-sulfur protein. *J. Biol. Inorg. Chem.* 7:632–39
107. Zu Y, Manon M-J, Couture MM-J, Kolling DRJ, Crofts AR, et al. 2003. The reduction potentials of Rieske clusters: the importance of the coupling between oxidation state and histidine protonation state. *Biochemistry.* In press
108. Hunte C. 2001. Insights from the structure of the yeast cytochrome bc_1 complex: crystallization of membrane proteins with antibody fragments. *FEBS Lett.* 504:126–32
109. de Vries S, Albracht SPJ, Leeuwerik FJ. 1979. The multiplicity and stoichiometry of the prosthetic groups in QH_2: cytochrome *c* oxidoreductase as studied by EPR. *Biochim. Biophys. Acta* 546:316–33
110. Ding H, Robertson DE, Daldal F, Dutton PL. 1992. Cytochrome bc_1 complex [2Fe-2S] cluster and its interaction with ubiquinone and ubihydroquinone at the Q_o site: a double-occupancy Q_o site model. *Biochemistry* 31:3144–58
111. Sharp RE, Palmitessa A, Gibney BR, White JL, Moser CC, et al. 1999. Ubiquinone binding capacity of the *Rhodobacter capsulatus* cytochrome bc_1 complex: effect of diphenylamine, a weak binding Q_o site inhibitor. *Biochemistry* 38:3440–46
112. Samoilova RI, Kolling D, Uzawa T, Iwasaki T, Crofts AR, Dikanov SA. 2002. The interaction of the Rieske iron sulfur protein with occupants of the Q_o-site of the bc_1 complex, probed by 1D and 2D

electron spin echo envelope modulation. *J. Biol. Chem.* 277:4605–8
113. Brandt U, Haase U, Schägger H, von Jagow G. 1991. Significance of the "Rieske" iron-sulfur protein for formation and function of the ubiquinol-oxidation pocket of mitochondrial cytochrome c reductase (bc_1 complex) *J. Biol. Chem.* 266:19958–64
114. Covián R, Pardo JP, Moreno-Sánchez R. 2002. Tight binding of inhibitors to bovine *bc*1 complex is independent of the Rieske protein redox state—consequences for semiquinone stabilization in the quinol oxidation site. *J. Biol. Chem.* 277:48449–55
115. Sharp RE, Gibney BR, Palmitessa A, White J, Dixon JA, et al. 1999. Effect of inhibitors on the ubiquinone binding capacity of the primary energy conversion site in the *Rhodobacter capsulatus* cytochrome bc_1 complex. *Biochemistry* 38:14973–80
116. Darrouzet E, Valkova-Valchanova M, Daldal F. 2002. The [2Fe-2S] cluster E_m as an indicator of the iron-sulfur subunit position in the ubihydroquinone oxidation site of the cytochrome bc_1 complex. *J. Biol. Chem.* 277:2464–70
117. Crofts AR, Shinkarev VP, Dikanov SA, Samoilova RI, Kolling D. 2002. Interactions of quinone with the iron-sulfur protein of the bc_1 complex: Is the mechanism spring-loaded? *Biochim. Biophys. Acta* 1555:48–53
118. Shinkarev VP, Kolling DRJ, Miller TJ, Crofts AR. 2002. Modulation of the midpoint potential of the [2Fe-2S] Rieske iron sulfur center by Q_o occupants in the bc_1 complex. *Biochemistry* 41:14372–82
119. Gatti DL, Meinhardt SW, Ohnishi T, Tzagoloff A. 1989. Structure and function of the mitochondrial bc_1 complex. A mutational analysis of the yeast Rieske iron-sulfur protein. *J. Mol. Biol.* 205:421–35
120. Denke E, Merbitzzahradnik T, Hatzfeld OM, Snyder CH, Link TA, Trumpower BL. 1998. Alteration of the midpoint potential of the Rieske iron-sulfur protein by changes of amino acids forming H-bonds to the iron-sulfur cluster. *J. Biol. Chem.* 273:9085–93
121. Schröter T, Hatzfeld OM, Gemeinhardt S, Korn M, Friedrich T, et al. 1998. Mutational analysis of residues forming hydrogen bonds in the Rieske [2Fe2S] cluster of the cytochrome bc_1 complex of *Paracoccus denitrificans*. *Eur. J. Biochem.* 255:100–6
122. Van Doren SR, Gennis RB, Barquera B, Crofts AR. 1993. Site-directed mutations of conserved residues of the Rieske iron-sulfur subunit of the cytochrome bc_1 complex of *Rhodobacter sphaeroides* blocking or impairing quinol oxidation. *Biochemistry* 32:8083–91
123. Yun C-H, Crofts AR, Gennis RB. 1991. Assignment of the histidine axial ligands to the cytochrome b_H and cytochrome b_L components of the bc_1 complex from *Rb. sphaeroides* by site-directed mutagenesis. *Biochemistry* 30:6747–54
124. Hacker B, Barquera B, Crofts AR, Gennis RB. 1993. Characterization of mutations in the cytochrome *b* subunit of the bc_1 complex of *Rhodobacter sphaeroides* that affect the quinone reductase site (Qc). *Biochemistry* 32:4403–10
125. Crofts AR, Barquera B, Bechmann G, Guergova M, Salcedo-Hernandez R, et al. 1995. Structure and function in the bc_1-complex of *Rb. sphaeroides*. In *Photosynthesis: From Light to Biosphere*, ed. P Mathis, 2:493–500. Dordrecht: Kluwer
126. Shinkarev VP, Crofts AR, Wraight CA. 2001. The electric field generated by photosynthetic reaction center induces rapid reversed electron transfer in the bc_1 complex. *Biochemistry* 40:12584–90
127. Davidson VL. 1996. Unraveling the kinetic complexity of inter-protein electron transfer reactions. *Biochemistry* 35:14036–39
128. Moser CC, Page CC, Farid R, Dutton PL. 1995. Biological electron transfer. *J. Bioenerg. Biomembr.* 27:263–74
129. Roberts JA, Kirby JP, Wall ST, Nocera

DG. 1997. Electron transfer within ruthenium(II) polypyridyl-(salt bridge)-dimethylaniline acceptor-donor complexes. *Inorgr. Chim. Acta* 263:395–405
130. Cukier RI, Nocera DG. 1998. Proton-coupled electron transfer. *Annu. Rev. Phys. Chem.* 49:337–69
131. Graige MS, Paddock ML, Feher G, Okamura MY. 1999. Observation of the protonated SQ intermediate in isolated reaction centers from *Rhodobacter sphaeroides*: implications for the mechanism of electron and proton transfer in proteins. *Biochemistry* 38:11465–73
132. Kresge AJ, Silverman DN. 1999. Application of Marcus Rate Theory to proton transfer in enzyme catalyzed reactions. *Methods Enzymol.* 308:276–97
133. Pines E, Magnes B-Z, Lang MJ, Fleming GR. 1997. Direct measurement of intrinsic proton transfer rates in diffusion controlled reactions. *Chem. Phys. Lett.* 281:413–20
134. Crofts AR. 2003. Proton-coupled electron transfer at the Q_o-site of the bc_1 complex controls the rate of ubihydroquinone oxidation. *Biochim. Biophys. Acta.* In press
135. Marcus RA, Sutin N. 1985. Electron transfers in chemistry and biology. *Biochim. Biophys. Acta* 811:265–322
136. Page CC, Moser CC, Chen XX, Dutton PL. 1999. Natural engineering principles of electron tunnelling in biological oxidation-reduction. *Nature* 402:47–52
137. DeVault D. 1980. Quantum-mechanical tunnelling in biological systems. *Q. Rev. Biophys.* 13:387–564
138. Xiao K, Yu L, Yu C-A. 2000. Confirmation of the involvement of protein domain movement during the catalytic cycle of the cytochrome bc_1 complex by the formation of an inter-subunit disulfide bond between cytochrome *b* and the iron-sulfur protein. *J. Biol. Chem.* 275:38597–604
139. Zhang L, Tai CH, Yu L, Yu C-A. 2000. pH-induced intramolecular electron transfer between the iron-sulfur protein and cytochrome c_1 in bovine cytochrome bc_1 complex. *J. Biol. Chem.* 275:7656–61
140. Starkov AA, Fiskum G. 2001. Myxothiazol induces H_2O_2 production from mitochondrial respiratory chain. *Biochem. Biophys. Res. Commun.* 281:645–50
141. Muller F, Crofts AR, Kramer DM. 2002. Multiple Q-cycle bypass reactions at the Q_o-site of the cytochrome bc_1 complex. *Biochemistry* 41:7866–74
142. Bartoschek S, Johansson M, Geierstanger BH, Okun JG, Lancaster CRD, et al. 2001. Three molecules of ubiquinone bind specifically to mitochondrial cytochrome bc_1 complex. *J. Biol. Chem.* 276:35231–34
143. Muller FL, Roberts AG, Bowman MK, Kramer DM. 2003. Architecture of the Q_o site of the cytochrome bc_1 complex probed by superoxide production. *Biochemistry* 42:6493–99
144. Crofts AR, Barquera B, Gennis RB, Kuras R, Guergova-Kuras M, Berry EA. 1999. Mechanistic aspects of the Q_o-site of the bc_1 complex as revealed by mutagensis studies, and the crystallographic structure. In *The Phototrophic Prokaryotes*, ed. GA Peschek, W Loeffelhardt, G Schmetterer, pp. 229–39. New York: Plenum
145. Slater EC. 1981. The cytochrome *b* paradox, the BAL-labile factor and the Q-cycle. In *Chemiosmotic Proton Circuits in Biological Membranes*, ed. VP Skulachev, PV Hinkle, pp. 69–104. Reading, MA: Addison-Wesley
146. Andrews KM. 1984. *Purification and characterization of the cytochrome* bc_1 *complex from* Rhodobacter sphaeroides. PhD thesis, Univ. Illin. Urbana-Champaign
147. Hunte C, Solmaz S, Lange C. 2002. Electron transfer between yeast cytochrome bc_1 complex and cytochrome *c*: a structural analysis. *Biochim. Biophys. Acta* 1555:21–28
148. Tian H, Sadoski R, Zhang L, Yu C-A, Yu L, Durham B, Millett F. 2000. Definition of the interaction domain for cytochrome

c on the cytochrome bc_1 complex. Steady-state and rapid kinetic analysis of electron transfer between cytochrome *c* and *Rhodobacter sphaeroides* cytochrome bc_1 surface mutants. *J. Biol. Chem.* 275:9587–95

149. Berry EA, Zhang Z, Huang L-S, Kim SH. 1999. Structures of quinone-binding sites in *bc* complexes: functional implications. *Biochem. Soc. Trans.* 27:565–72
150. Berry EA, Huang L-S, Zhang Z, Kim SH. 1999. Structure of the avian mitochondrial cytochrome bc_1 complex. *J. Bioenerg. Biomembr.* 31:177–90
151. Zhang Z-L, Berry EA, Huang L-S, Kim S-H. 2000. Mitochondrial cytochrome bc_1 complex. *Subcell. Biochem.* 35:541–80
152. Brasseur G, Sami Saribas A, Daldal F. 1996. A compilation of mutations located in the cytochrome *b* subunit of the bacterial and mitochondrial bc_1 complex. *Biochim. Biophys. Acta* 1275:61–69
153. Iwata M. 2001. *Structural studies on cytochrome* bc_1 *complex from bovine heart mitochondria*. PhD diss. Uppsala Univ., Sweden
154. Ohnishi T, Trumpower BL. 1980. Differential effects of antimycin on ubisemiquinone bound in different environments in isolated succinate cytochrome *c* reductase complex. *J. Biol. Chem.* 255:3278–84
155. Robertson DE, Prince RC, Bowyer JR, Matsuura K, Dutton PL, Ohnishi T. 1984. Thermodynamic properties of the semiquinone and its binding site in the ubiquinol:cytochrome $c(c_2)$ oxidoreductase of respiratory and photosynthetic systems. *J. Biol. Chem.* 259:1758–63
156. de la Rosa FF, Palmer G. 1983. Reductive titration of CoQ-depleted Complex III from baker's yeast: evidence for an exchange-coupled complex between $QH^{\bullet}$ and low-spin ferricytochrome b. *FEBS Lett.* 163:140–43
157. Salerno JC, Osgood M, Liu Y, Taylor H, Scholes CP. 1990. Electron nuclear double resonance (ENDOR) of the Q-c.-ubiSQ radical in the mitochondrial electron transport chain. *Biochemistry* 29:6987–93
158. Kolling DRJ, Samoilova RI, Holland JT, Berry EA, Dikanov SA, Crofts AR. 2003. Exploration of ligands to the Q_i-site semiquinone in the bc_1 complex using high-resolution EPR. *J. Biol. Chem.* 278:39747–54
159. Hacker B, Barquera B, Gennis RB, Crofts AR. 1994. Site-directed mutagenesis of arginine-114 and tryptophan-129 in the cytochrome *b* subunit of the bc_1 complex of *Rhodobacter sphaeroides*: two highly conserved residues predicted to be near the cytoplasmic surface of putative transmembrane helices B and C. *Biochemistry* 33:13022–31
160. Salerno JC, Xu Y, Osgood P, Kim CH, King TE. 1989. Thermodynamic and spectroscopic characteristics of the cytochrome bc_1 complex. Role of quinone in the behavior of cytochrome b_{562}. *J. Biol. Chem.* 264:15398–403
161. Rich PR, Jeal AE, Madgwick SA, Moody AJ. 1990. Inhibitor effects on redox-linked protonations of the *b* hemes of the mitochondrial bc_1 complex. *Biochim. Biophys. Acta* 1018:29–40
162. Zweck A, Bechmann G, Weiss H. 1989. The pathway of the quinol/quinone transhydrogenation reaction in ubiquinol: cytochrome-*c* reductase of *Neurospora* mitochondria. *Eur. J. Biochem.* 183:199–203
163. Rich PR, Madgwick SA, Moss DA. 1991. The interactions of duroquinol, DBMIB and NQNO with the chloroplast cytochrome bf complex. *Biochim. Biophys. Acta* 1058:312–28
164. Dutton PL, Wilson DM. 1976. Redox potentiometry in biological systems. *Methods Enzymol.* 54:411–35
165. Glaser EG, Meinhardt SW, Crofts AR. 1984. Reduction of cytochrome b_{561} through the antimycin-sensitive site of the ubiquinol:cytochrome c_2 oxidoreductase

complex of *Rps. sphaeroides*. *FEBS Lett.* 178:336–42

166. Gray KA, Dutton PL, Daldal F. 1994. Requirement of histidine-217 for ubiquinone reductase activity (Q_i-site) in the cytochrome-bc_1 complex. *Biochemistry* 33:723–33
167. Dutton PL, Jackson JB. 1972. Thermodynamic and kinetics characterization of electron-transfer components in situ in *Rps. spheroides* and *Rhodospirillum rubrum*. *Eur. J. Biochem.* 30:495–510
168. Meinhardt SW, Crofts AR. 1984. A new effect of antimycin on the *b*-cytochromes of *Rps. sphaeroides*. In *Advances in Photosynthesis Research*, ed. C Sybesma, 1:649–52. The Hague: Nijhoff/Junk
169. Hacker B. 1994. *Mutational studies of the cytochrome bc_1 complex of* Rhodobacter sphaeroides. PhD thesis, Univ. Illinois, Urbana-Champaign. 94 pp.
170. Snyder CH, Trumpower BL. 1999. Ubiquinone at center n is responsible for triphasic reduction of cytochrome *b* in the cytochrome bc_1 complex. *J. Biol. Chem.* 274:31209–16
171. Bechmann G, Weiss H, Rich PR. 1992. Non-linear inhibition curves for tight-binding inhibitors of dimeric ubiquinol-cytochrome c oxidoreductases. Evidence for rapid inhibitor mobility. *Eur. J. Biochem.* 208(2):315–25
172. Rich PR, Bendall DS. 1980. The kinetics and thermodynamics of the reduction of cytochrome *c* by substituted p-benzoquinols in solution. *Biochim. Biophys. Acta* 592:506–18

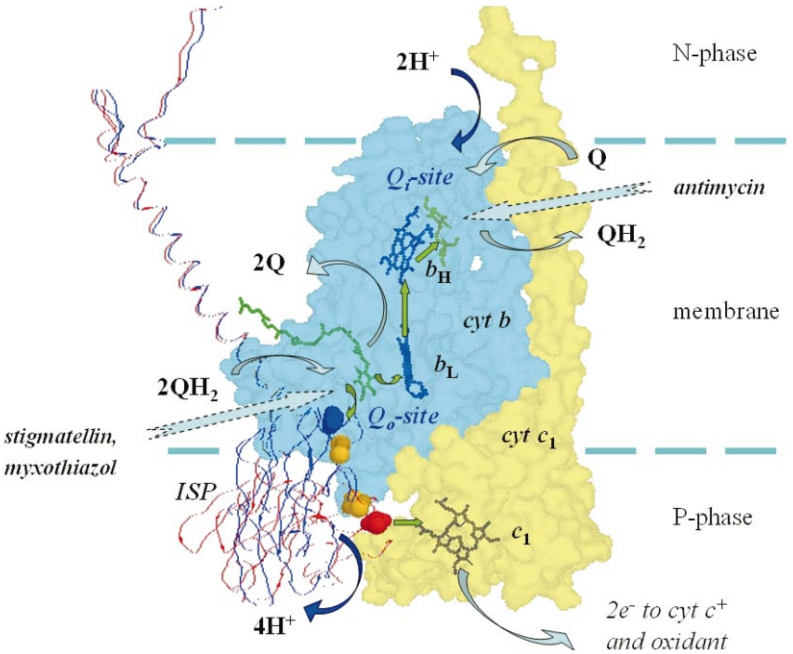

$$QH_2 + 2\ \text{cyt c}^+ + 2H_N^+ \leftrightarrows Q + 2\ \text{cyt c} + 4H_P^+$$

Figure 1 The Q-cycle mechanism shown in the context of a functional monomer. The three catalytic subunits of the bc_1 complex (PDB 2bcc) from chicken mitochondria are shown with a quinol modeled in the Q_o-site to replace stigmatellin, and quinone at the Q_i-site. The cyt *b* subunit is shown by its transparent cyan surface, and the cyt c_1 subunit by a transparent yellow surface. The Rieske iron sulfur protein is shown as a ribbon cartoon, docked at the *b*-interface (*blue*) or at the *c*-interface (*red*). The approximate position of the membrane is shown by the dashed lines. The *b*-hemes are shown in blue, heme c_1 in green. The [2Fe-2S] clusters are shown as space-filling models, colored as for the protein. Two additional positions for the cluster are shown (in *CPK colors*) to indicate the trajectory of movement between *b*- and *c*-interfaces. Binding and unbinding of quinone species, and docking of cyt *c*, are shown by broad curved arrows (*light-blue*). Electron transfers are shown by small green arrows, H^+ release and uptake are shown by curved blue arrows. The sites of action of inhibitors are shown by dotted light-blue arrows. For each turnover, two QH_2 molecules are oxidized to Q at the Q_o-site, and two successive electrons are passed down the pathways indicated by the green arrows. The two electrons going down the high-potential chain (ISP, cyt c_1, cyt *c*) are passed to a terminal oxidant. The two electrons going through the *b*-heme chain reduce Q to QH_2 at the Q_i-site through a two-electron gate, with storage of one electron as a SQ at the site.

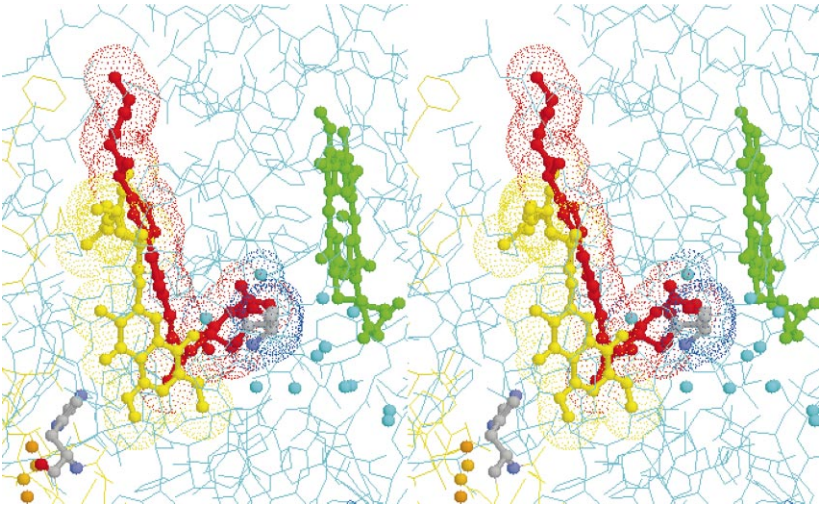

Figure 2 Stigmatellin and myxothiazol at the Q_o-site. The stigmatellin-containing structure of the bovine mitochondrial complex (PDB 1pp9) shows the positions of His-161 of ISP (*ball and stick model, bottom left*) and Glu-271 of cyt *b* (*center*, both in CPK colors) acting as ligands to the stigmatellin (yellow ball & stick model). The rest of the protein is represented by a wire-frame model, with cyt *b* in cyan and ISP in yellow. Two waters that H-bond to Glu-272 and waters contributing to the chain leading to the external P-phase are shown as small cyan spheres. Heme b_L is shown as a green ball and stick model. Superimposed on this structure is myxothiazol (*red ball and stick model*) to show the position relative to heme b_L in a separate structure. A dotted surface at the van de Waals radii is shown for stigmatellin (*yellow dots*), myxothiazol (*red dots*), and Glu-271 together with its two H-bonded waters (*blue dots*). The almost complete overlap of Glu-271 and its waters with the pharmacophore of myxothiazol (the horizontal arm of the "L" of myxothiazol) can best be appreciated by stereo viewing (stereo model is set up for crossed-eye viewing).

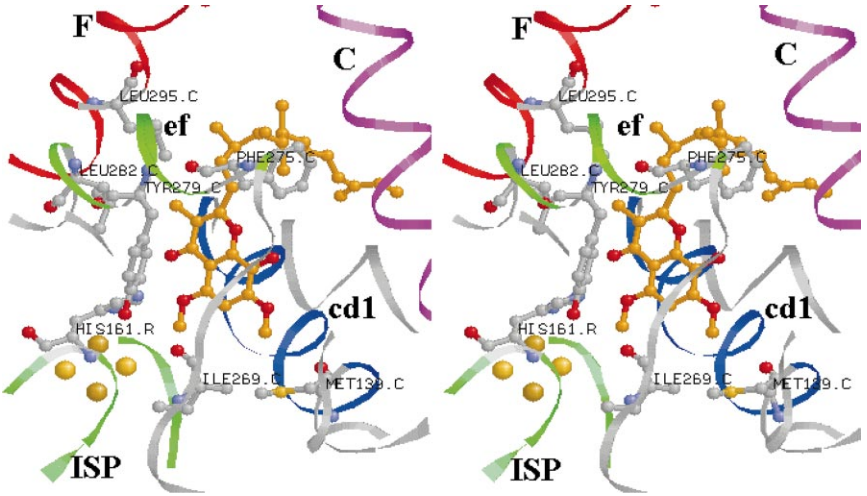

Figure 3 Residues modified in *P. falciparum* strains that are resistant to atovaquone. The residues are shown as ball and stick models in CPK coloring in the context of the stigmatellin structure, to show the binding of a similar occupant. The spans of cyt *b* contributing to the Q_o-site surface are shown as ribbons, with spans forming the Q_o-site binding domain identified as ribbon models of different colors. His-161 of ISP, the [2Fe-2S] cluster, and parts of the ISP protein (*green-blue ribbon*, *lower left*) are also shown. Stereo pair for crossed-eye viewing.

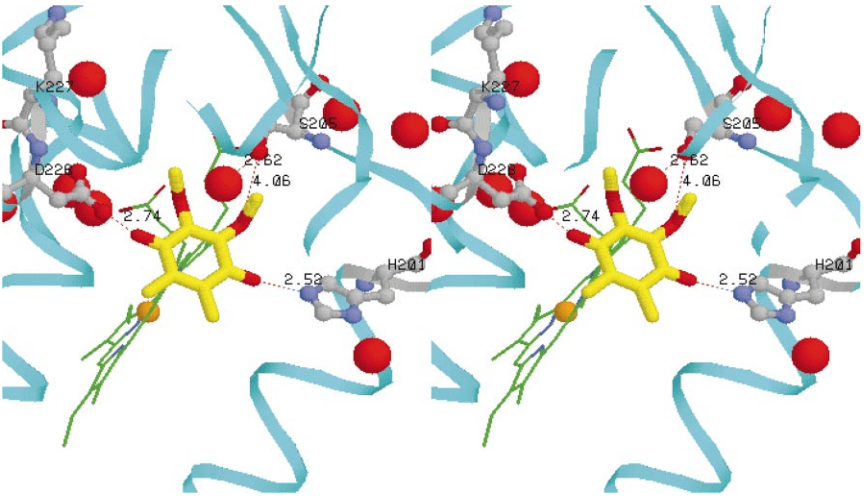

Figure 4 The liganding of quinone at the Q_i-site. The structure from Berry's bovine mitochondrial complex at 2.1 Å resolution (PDB 1pp9, 158) is shown, with potential H-bonding ligands to the quinone, and water molecules within 10.0 Å. The quinone is shown as a stick model, colored in CPK, but with C-atoms in yellow. Side chains involved as ligands are shown as ball and stick models in CPK colors. Distances shown are in Å. The rest of the protein close to the site is represented by a blue ribbon. Heme b_H is shown as a skinny stick model in CPK colors, with C-atoms in green. Water O-atoms are shown by larger red spheres. Stereo image for crossed-eyed viewing.